Effect of imperfections on the actuation performance of lattice materials

Gençoğlu, C.; Tekoğlu, C.; Ayas, C.

DOI
10.1016/j.ijsolstr.2022.111779

Publication date
2022

Document Version
Final published version

Published in
International Journal of Solids and Structures

International Journal of Solids and Structures 252 (2022) 111779

Contents lists available at ScienceDirect

International Journal of Solids and Structures

journal homepage: www.elsevier.com/locate/ijsolstr

Effect of imperfections on the actuation performance of lattice materials

C. Gençoğlu [a], C. Tekoğlu [a,*], C. Ayas [b]

[a] Department of Mechanical Engineering, TOBB University of Economics and Technology, Söğütözü, Ankara, 06560, Turkey
[b] Structural Optimisation and Mechanics Group, Department of Precision and Microsystems Engineering, Faculty of Mechanical, Maritime and Material Engineering, Delft University of Technology, Mekelweg 2, Delft, 2628 CD, The Netherlands

ARTICLE INFO

Keywords:
Lattice materials
Morphing structures
Actuation
Mechanical properties
Finite element analysis

ABSTRACT

The effects of five different types of imperfection (fractured cell walls, missing cells, cell wall waviness, cell wall misalignment, and non-uniform cell wall thickness) on actuation performance are numerically investigated for the Kagome lattice and two of its variants: Double Kagome (DK) and Kagome with concentric triangles (KT). The lattice materials of interest are excited by deploying a single linear actuator located at their centre. The actuation performance of the lattices is determined by measuring the energy spent by the actuator and the attenuation distance of the deformation induced by the actuator. The deformation localises in a narrow corridor approximately one unit cell-wide for all three lattices in the absence of imperfections. The finite element calculations show that the critical parameter determining the actuation performance is the stiffness along the actuation corridor rather than the macroscopic Young's modulus of the lattice. The less stiff the actuation corridor is, the smaller the actuation energy and the larger the attenuation distance (except when there is a fractured or wavy cell wall or a missing cell along the actuation corridor that immediately attenuates the displacement field). When imperfections are randomly distributed outside the actuation corridor, cell wall misalignment and non-uniform cell wall thickness barely affect the actuation performance, although cell wall misalignment considerably reduces the macroscopic Young's modulus of the lattice. The actuator feels the presence of fractured or wavy cell walls or missing cells, whether placed inside or outside the actuation corridor. These three types of imperfection cause the largest knock-down both in the macroscopic Young's modulus of the block and the actuation energy while increasing the attenuation distance. The increase in the attenuation distance due to imperfections is, however, impotent, as the accompanying reduction in stiffness makes the lattice more vulnerable to failure. However, if a defect is introduced slightly beyond the attenuation distance of the perfect lattice as an intentional design feature, it is beneficial for the actuation performance without decreasing the macroscopic Young's modulus.

1. Introduction

Lattice materials are a subclass of cellular materials with a repetitive structure. In this paper, we study lattice materials comprising a network of slender beams (struts) meeting at lattice points. The repetitive nature of the lattice materials is described by a periodic unit cell that tessellates the plane or space for 2D and 3D lattice materials, respectively. The term material emphasises that the global dimensions of the lattice and the wavelengths of the loadings it is subjected to are orders of magnitude larger than those of the unit cell, leading to the separation of length scales. Consequently, a lattice material can be treated as a continuum with macroscopic properties such as Young's modulus and yield strength (e.g., Onck et al., 2005). If a lattice does not satisfy this condition, it behaves like a structure. The macroscopic properties of a lattice material depend on (i) the relative density (the volume fraction of beams), (ii) the material properties of the strut material, and (iii) the geometric layout and the connectivity of the beams within the unit cell that is also commonly called the micro-architecture.

Lattice materials have been of interest in creating shape morphing structures through actuation with application areas such as morphing aircraft wings (e.g., Bornengo et al., 2005; Olympio and Gandhi, 2010; Namasivayam and Seepersad, 2011; Cheung et al., 2017; Jenett et al., 2017) and lightweight deployable booms and antennas (e.g., De-Nicola et al., 2021; McHale et al., 2021). Extensive reviews on lattice (and other smart) materials in morphing applications are given by, for example, (Daynes and Weaver, 2013) and Sun et al. (2016). A shape morphing lattice material is typically attained by replacing a few lattice members (struts, cell walls) with actuators that can extend or shorten in response to an external stimulus (e.g., Donev and Torquato, 2003;

* Corresponding author.
E-mail address: cihantekoglu@etu.edu.tr (C. Tekoğlu).

https://doi.org/10.1016/j.ijsolstr.2022.111779
Received 17 January 2022; Received in revised form 9 May 2022; Accepted 3 June 2022
Available online 9 June 2022

dos Santos e Lucato et al., 2004; Fleck et al., 2010), e.g., temperature change or electrical potential difference. Depending on the micro-architecture, the deformation initiated by the actuator can propagate over a large area/volume of the lattice leading to a desired shape change.

A lattice micro-architecture ideal for actuation exhibits (i) isotropic elasticity, (ii) a high stiffness against external loads in the absence of actuation, and (iii) a compliant response to actuation. The first condition necessitates the micro-architecture of the lattice to have a sufficient degree of structural symmetry, e.g., three-fold or six-fold symmetry for in-plane isotropy in a 2D lattice (Ayas and Tekoğlu, 2018). Because the axial stiffness of slender members is significantly higher than their bending stiffness, simultaneous fulfilment of the remaining two conditions requires stretching-dominated deformation of lattice members against external loads in the absence of actuation and bending-dominated deformation of lattice members during actuation.

Lattice materials, by definition, consist of a large number of members and thus can be treated as infinitely large periodic networks of rigidly jointed struts (Deshpande et al., 2001). Therefore, stretching-dominated elastic deformation of a lattice material can be traced back to the rigidity of the repetitive (infinite) pin-jointed truss with identical micro-architecture. The equilibrium for a periodic unit cell of a repetitive truss can be stated as $\mathbf{At} = \mathbf{f}$ where $\mathbf{A}$ is the equilibrium matrix, $\mathbf{t}$ is the array of bar tensions of the members within the unit cell, and $\mathbf{f}$ is the array of nodal force components in the x_1 and x_2 directions for the joints within the unit cell. The non-zero solutions of $\mathbf{t}$ to $\mathbf{At} = \mathbf{0}$ correspond to states of self-stress that arise in response to the macroscopic remote stresses applied at infinity, not to any particular node of the repetitive truss (Guest and Hutchinson, 2003). A repetitive truss is then rigid if it exhibits states of self-stress that sustain all macroscopic remote loading possibilities. In 2D, the three possible types of macroscopic loading are tension/compression in the x_1 and x_2 directions and shear in the $x_1 - x_2$ plane. Therefore, the minimum number of linearly independent states of self-stress s that can render a 2D repetitive pin-jointed truss rigid is $s = 3$ (Guest and Hutchinson, 2003). Similarly, bending-dominated elastic deformation of a lattice micro-architecture during actuation can be traced back to the lack of rigidity of the equivalent repetitive pin-jointed truss. The simplest case of single-member actuation corresponds to removing a member from the truss and applying point forces at the two joints at which the missing member was connected, triggering an inextensional collapse mechanism. These two distinct modes of deformation in the absence and presence of actuation can only be achieved if the repetitive pin-jointed micro-architecture in the passive (not actuated) state is "just rigid". A finite truss can be "just rigid" if it is both kinematically and statically determinant, possessing neither any collapse mechanisms nor any states of self-stress, i.e. satisfies the Maxwell–Calladine condition (Maxwell, 1864; Calladine, 1978; Pellegrino and Calladine, 1986). An infinite repetitive truss, on the other hand, cannot be both statically and kinematically determinant (Guest and Hutchinson, 2003) but still can be "just rigid" as long as it satisfies the Maxwell–Calladine condition[1] which implies $s = m$ (Guest and Hutchinson, 2003) where m denotes the number of inextensional collapse mechanisms. For a planar (2D) repetitive lattice, the Maxwell–Calladine condition is satisfied if the degree of nodal connectivity, i.e., the number of members attached to each joint is 4. Fulfilling the Maxwell–Calladine condition in addition to rigidity can then be further specified in 2D as $s = m \geq 3$ (Guest and Hutchinson, 2003; Hutchinson and Fleck, 2006; Nelissen et al., 2019). Consequently, the m inextensional mechanisms ($m \geq 3$) correspond to translation in x_1 and x_2 directions in addition to $m - 2 \geq 1$ non-strain- producing collapse mechanism(s). A non-strain-producing mechanism cannot be excited by any state of uniform macroscopic strain. Therefore, the presence of only non-strain producing collapse mechanism(s) is the ramification of the 2D repetitive truss being "just rigid". The presence of strain-producing mechanisms, on the other hand, is an indication of the lack of rigidity (Pronk et al., 2017). Non-strain-producing mechanism(s) of the "just rigid" repetitive truss with a member replaced by an actuator can be triggered under the local actuation forces. Thus, deploying an actuator can induce bending-dominated deformation in the corresponding lattice material with welded joints.

The recent advent in additive manufacturing technology reinvigorated the interest in lattice materials. Additive manufacturing and especially laser powder bed fusion (LPBF) (Gibson et al., 2021) enabled the realisation of lattice materials with highly intricate geometries, with (sub)millimetre scale cell wall (strut) dimensions from a multitude of metals and alloys, (e.g., Yan et al., 2012). Nevertheless, the lack of process robustness, stability, and repeatability are still points of concern leading to imperfections in additively manufactured lattice materials (Grasso and Colosimo, 2017; Echeta et al., 2020). In LPBF, a high-energy laser beam moving over the powder bed with a small spot radius melts and fuses the solid powder particles, creating a melt pool that subsequently solidifies. The heating–cooling cycles experienced at every material point are thus critical for the final quality of the lattice material. Overheating (Mertens et al., 2014) or incomplete fusion (Galy et al., 2018) can lead to strut over-sizing and under-sizing, respectively. Furthermore, dimensional inaccuracies in strut thickness are significantly affected by strut orientation with respect to the built direction. Struts oriented in the build direction are predisposed to under-sizing, while struts orthogonal to the build direction are vice versa (Cuadrado et al., 2017). This can lead to non-uniform cell wall thickness and, in the extreme, fractured cell walls. Moreover, Melancon et al. (2017) and Liu et al. (2017) observed deviations in the position of axes of the struts, defining this deviation as cell wall waviness. Metal additive manufacturing is also prone to generating residual stresses that are yet another source of imperfections. Residual stress arises due to the high thermal gradients and cooling rates within the part, subjecting the part to rapid thermal expansion and contraction. Consequently, residual stresses also act as a formation mechanism for imperfections such as misalignment, waviness, and fracture of cell walls (Echeta et al., 2020).

The influence of morphological imperfections, including those mentioned above, on the yielding of 2D cellular solids, has been studied by Chen et al. (1999). The imperfection sensitivity of in-plane elastic modulus and fracture toughness is explored for a range of lattice micro-architectures by Romijn and Fleck (2007). The study revealed that the reduction in stiffness and toughness are the most sensitive to the presence of imperfections for the Kagome and square lattices; see also Tankasala et al. (2017), where geometrical nonlinearities are also taken into account. Although the effects of fractured cell walls, missing cells, cell wall waviness, cell wall misalignment, and non-uniform wall thickness (the most commonly observed imperfections and thus the focus of this study) on the elastic, yield, buckling, localisation, and collapse behaviour of several two- and three-dimensional lattice materials have been extensively studied (e.g., Guo et al., 1994; Silva and Gibson, 1997; Guo and Gibson, 1999; Wallach and Gibson, 2001; Symons and Fleck, 2008; Lu et al., 2011; Gross et al., 2019), their effect on the actuation performance of lattice materials has not been thoroughly investigated. Change in the resistance to actuation of double-layer Kagome grid lattice material has been experimentally investigated for cell wall waviness by Symons et al. (2005). They concluded that wavy struts had a significant effect on actuation stiffness. However, a study covering several different lattice micro-architectures and investigating various types of imperfections commonly encountered in metal additive manufacturing has not yet been performed.

The Kagome lattice has been established as an excellent micro-architecture for actuation (e.g., Hyun and Torquato, 2002; Hutchinson et al., 2003). In the literature, no other lattice material has been proposed as an alternative to the Kagome lattice to be used as a stiff actuator until the recent work by Nelissen et al. (2019). Pronk

[1] This is a necessary but not sufficient condition for a repetitive truss to be "just rigid" (Pronk et al., 2017).

et al. (2017) proposed a set of criteria for a lattice to be suitable for actuation based on the states of self stress and mechanisms of the pin-jointed version of the lattice material. Nelissen et al. (2019) refined the set of criteria by Pronk et al. (2017) and designed Double Kagome (DK) and Kagome with concentric triangles (KT) as alternative lattice materials to the Kagome lattice in shape morphing applications. As the Kagome lattice, the DK lattice also satisfies the Hashin and Shtrikman (1963), Hashin (1965), Gurtner and Durand (2014) upper bounds for the elastic moduli of low-density elastic networks. Furthermore, single-member actuation in a DK lattice requires less energy than in a Kagome lattice, albeit actuation-induced deformations in a DK lattice attenuate more quickly. Despite having a lower passive stiffness, the KT lattice surpasses both the Kagome and DK lattices in terms of actuation performance. Even though the DK and KT lattices have proven to be among the best alternatives to the Kagome lattice for actuation in the absence of imperfections (Nelissen et al., 2019), imperfections in actual materials are unavoidable and can significantly alter the mechanical response. With this in mind, the goal of this research is to look at the actuation capabilities as well as the passive stiffness of Kagome, DK, and KT lattice micro-architectures in the presence of the five most frequently observed imperfections: fractured cell walls, missing cells, cell wall waviness, cell wall misalignment, and non-uniform wall thickness. We performed finite element calculations to systematically assess the passive macroscopic elastic modulus and the actuation performance of lattice materials with a random distribution of imperfections. In addition, we have also investigated the inclusion of a single imperfection along the actuation path as a design feature to enhance the actuation performance without compromising the passive stiffness.

2. Methods

This section explains the problem definition, the finite element (FE) model, and how the imperfections of interest are incorporated into the FE model.

2.1. Definition of the problem

Fig. 1 shows the three lattice micro-architectures investigated in this study: Kagome, Double Kagome (DK), Kagome with concentric triangles (KT), and the associated unit cells. Here the aim is to assess the stiffness and actuation performance of these three lattice micro-architectures in the presence of imperfections. For this purpose, a 2D rectangular block of lattice material containing a linear actuator at its geometric centre is employed, as schematically shown in Fig. 2. The block has a height of $H \approx 30\sqrt{3}\ l_0$ and a length of $L \approx 800\ l_0$, where $2l_0 = 2.0$ mm is the unit cell width for the three lattices. The linear actuator replaces a single cell wall for the Kagome and DK lattices and two cell walls for the KT lattice, as shown with the dashed lines in Fig. 1a–c. When the actuator is extended, the struts of the lattice deform, and for an imperfection-free lattice, the deformation is confined to the region denoted *actuation corridor* in Fig. 2. The actuation corridor for each lattice micro-architecture is indicated with red dotted lines in Fig. 1 and has a height of $h_c \approx \sqrt{3}\ l_0$ for the Kagome and KT lattices, and $h_c \approx 2.1\ l_0$ for the DK lattice.

In this study, the actuation performance of a lattice material is quantified by two different measures. The first is the *actuation energy*, defined as the energy consumed by a single linear actuator stretched to an actuation strain of ε_a (see also Wicks and Guest, 2004; Nelissen et al., 2019). The second is the *attenuation distance*, defined as the distance from the tip of the actuator to the point where the displacement (in the actuation direction) imposed by the actuator reduces to 20% of its value at the tip (see also Wicks and Guest, 2004; Nelissen et al., 2019). Generally speaking, the lower the actuation energy, the longer the attenuation distance, and the better the actuation performance of a lattice material.

Table 1
Relative densities ($\bar{\rho}$) of the considered lattices in terms of the in-plane cell wall thickness (t_{in}) and unit cell width ($2l_0$), see Fig. 1.

Structure	Kagome	DK	KT
$\bar{\rho}$	$\sqrt{3}\frac{t_{in}}{l_0}$	$2\sqrt{3}\frac{t_{in}}{l_0}$	$\frac{3}{2}\sqrt{3}\frac{t_{in}}{l_0}$

The attenuation distance is severely reduced by the presence of an imperfection in the actuation corridor, whether the lattice contains additional imperfections outside the corridor or not. This study is therefore divided into two parts. In the first part, we consider an intentional placement of a single imperfection as a design feature in the actuation corridor at a certain distance from the tip of the actuator, while the remaining regions of the lattice block are left imperfection free (see Section 3.1). In the second part, the actuation corridor and the rectangular region with dimensions $h_a \times l_a$ (where $h_a = 8\sqrt{3}l_0$ and $l_a = 10l_0$) containing the actuator are left imperfection-free.[2] However, a certain number of imperfections are randomly distributed in the *imperfection zone* with length l depicted in Fig. 2 (see Section 3.2).

2.2. Finite element (FE) model

In the FE calculations, the cell walls (struts) of all three lattice micro-architectures are assumed to have a rectangular cross-section with an out-of-plane thickness of $t_{out} = 0.01$ mm. For the Kagome and KT micro-architectures, all the cell walls have the same length, while for the DK micro-architecture, there are two families of cell walls, each with a different length. As the unit cell width is taken to be $2l_0 = 2.0$ mm for all three structures (see Fig. 1), the cell wall length becomes $l_{cw} = 1.0$ mm for the Kagome, $l_{cw} = 0.5$ mm for the KT, and $l_{cw1} = 0.4$ and $l_{cw2} = 0.8$ mm for the DK lattices. The in-plane cell wall thickness, t_{in}, for each lattice is calculated using the relative density (which corresponds to the volume fraction of the cell walls) expressions given in Table 1. For the above given dimensions and a relative density of $\bar{\rho} = 0.01$, $t_{in} = 0.005773$ mm for the Kagome, $t_{in} = 0.003849$ mm for the KT, and $t_{in} = 0.002887$ mm the DK micro-architecture.

The resistance of a lattice material to actuation is here quantified by the energy consumed by a single linear actuator replacing a cell wall of the lattice as in Wicks and Guest (2004) and Nelissen et al. (2019). The energy consumed by the linear actuator for an actuation strain of ε_a, i.e., the work done by the actuator during its extension, is

$$W = -\frac{1}{2} t \lambda \varepsilon_a, \tag{1}$$

where λ is the undeformed actuator length and t is the tension in the actuator in the deformed configuration, where $t < 0$ for $\varepsilon_a > 0$. A normalised value for the actuation energy, $\hat{W} = W/W_0$, is also defined, with W_0 as the energy consumed by the actuator when the lattice is free of imperfections. The actuator is assumed to have the same geometric and material properties as the regular cell walls of the lattice.

Fig. 3 shows the FE mesh and the boundary conditions (BCs) for a Kagome lattice block to be deformed by a single linear actuator located at its geometric centre. The empty circles in this example denote the location of the fractured cell walls, which are removed from the mesh. Note that no imperfection is placed in the actuator corridor, indicated by the two dashed lines, or the rectangular region surrounding the actuator, indicated by the solid red lines, see also Fig. 2. Displacement BCs are applied to the two ends of the actuator (indicated by two arrows with opposing directions) such that the strain in the actuator becomes $\varepsilon_a > 0$. All three active degrees of freedom – the two in-plane displacements and the single in-plane rotation – are fixed for all

[2] The presence of imperfections in this zone prevents the actuator from imposing a notable deformation on the lattice.

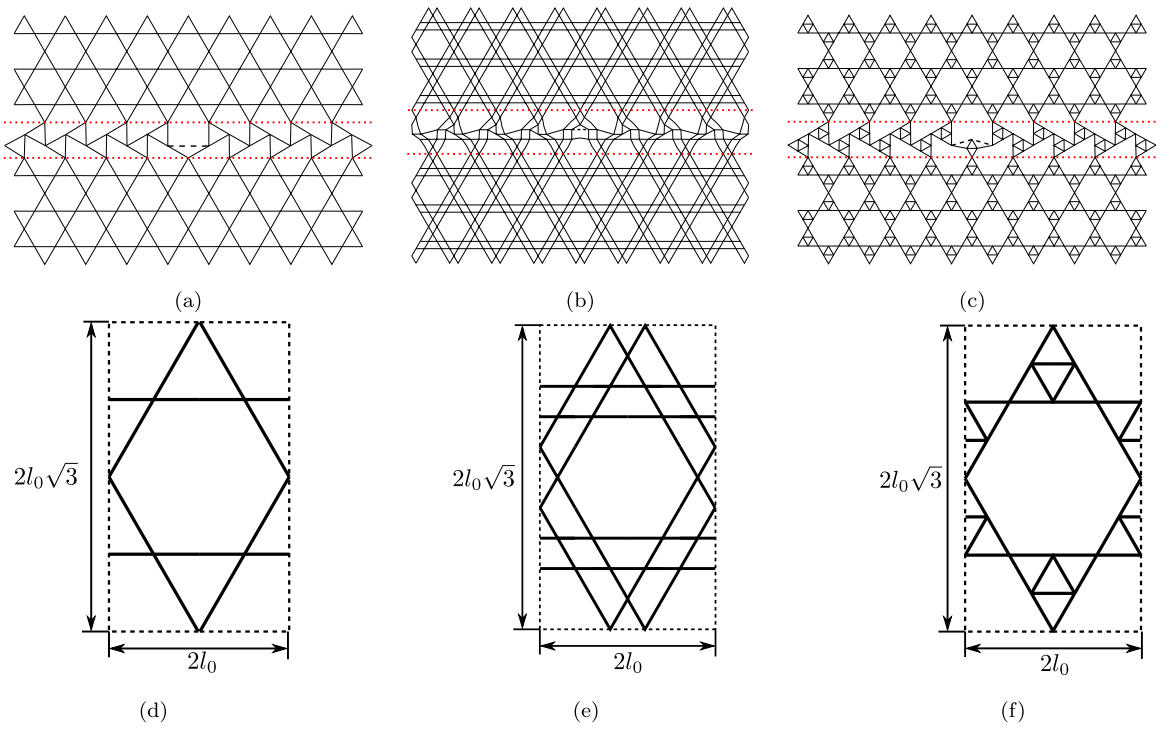

Fig. 1. Lattice materials investigated in this study (a, b, c) and their unit cells (d, e, f): (a, d) Kagome, (b, e) Double Kagome (DK), (c, f) Kagome with concentric triangles (KT). In (a, b, c), the dashed lines represent a linear actuator and the dotted lines the top and bottom boundaries of the actuation corridor. The linear actuator replaces a single cell wall for the Kagome and DK lattices, and two cell walls for the KT lattice. The actuation corridor has a height of $h_c \approx \sqrt{3}\ l_0$ for the Kagome and KT lattices, and $h_c \approx 2.1\ l_0$ for the DK lattice. In (d, e, f), the dashed lines indicate the unit cell boundaries.

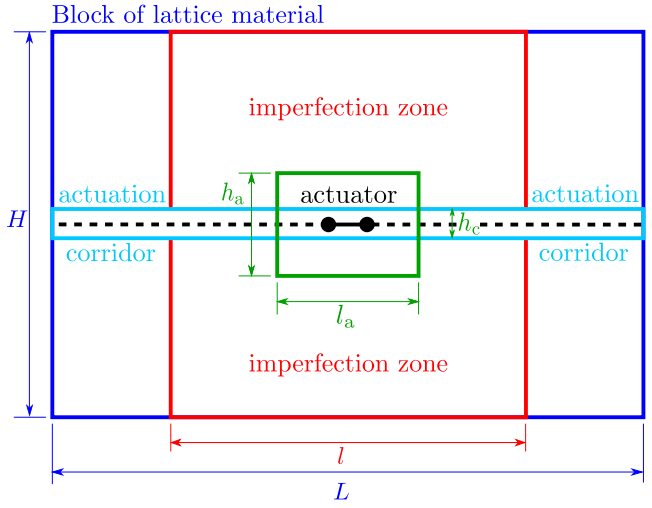

Fig. 2. Schematic showing the different zones in the material block employed to measure the actuation performance of the lattices presented in Fig. 1. Either a single imperfection (see Fig. 4) is placed in the "actuation corridor", over the cell walls sitting on the horizontal dashed line passing through the actuator, or $f\%$ imperfections are randomly distributed within the two areas denoted "imperfection zone". In both cases, the close vicinity of the actuator (the rectangular region $h_a \times l_a$) is left imperfection-free.

the external boundary nodes. The actual lattice block used in the FE calculations is much larger than the one shown in Fig. 3 for illustration purposes; see Section 2.1. In fact, the dimensions of the lattice block are chosen such that fully clamped and traction-free BCs at the outer edges of the block yield nearly identical $\hat{W}$ values, which implies that the boundary effects play a minor role in the actuation behaviour of the lattice. Consequently, only the results for fully clamped BCs are presented in the remainder. The macroscopic Young's modulus of the lattice block is calculated by imposing uniaxial compression BCs. Note that the size of the lattice block is also much larger than the dimensions of the unit cell to treat the lattice as a material with homogenised macroscopic properties. We note that all three lattice micro-architectures are governed by isotropic elasticity due to 3-fold structural symmetry, see e.g., Ayas and Tekoğlu (2018).

The FE analyses are carried out using the commercial software (Abaqus, 2020). Lattice materials are most often loaded in the elastic deformation regime (e.g., Symons and Fleck, 2008). Therefore, all the FE calculations are performed in the linear elastic regime, and geometric nonlinearities are disregarded. The cell walls of the lattice materials are modelled with two-noded cubic Euler–Bernoulli beam elements (element B23 in Abaqus (2020)), which can deform axially and bend but do not allow for shear deformation. Imperfection-free and misaligned cell walls are meshed with a single element, while 18 and 8 elements are used respectively for wavy cell walls and cell walls with a non-uniform thickness. The cell wall material properties are taken as Young's modulus of $E_s = 70$ GPa and a Poisson ratio of $\nu = 0.33$, representative of aluminium alloys. However, although the quantitative results are sensitive to the choice of the cell wall material, the tendencies described subsequently would remain the same upon changing elastic material properties.

2.3. Types of imperfections

Five different types of imperfections are considered, as schematically illustrated in Fig. 4: (a) fractured cell wall, (b) missing cell, (c) cell wall waviness, (d) cell wall misalignment, and (e) non-uniform cell wall thickness. In (b), the missing cell in the Kagome, DK, and KT lattices is shown with encircled dashed lines. Fractured cell walls and missing cells are simply removed from the FE mesh. Cell wall waviness is modelled by imposing an initial transverse deflection on the nodes of the beam elements through a sinusoidal wave function given as

$$y(x) = A \sin\left(\frac{2\pi f x}{l_{cw}}\right), \tag{2}$$

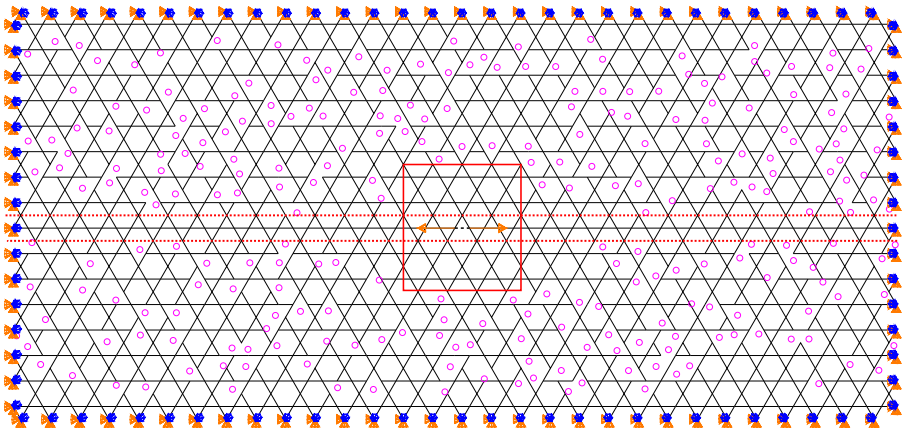

Fig. 3. The FE mesh and the boundary conditions for the Kagome lattice containing a single linear actuator in its geometric centre. The empty circles denote the location of the fractured cell walls, which are simply removed from the mesh. The two arrows with opposing directions indicate the displacement boundary conditions imposed on the actuator, and dotted lines represent the top and bottom boundaries of the actuation corridor. All the external boundary nodes of the lattice are clamped by fixing the two in-plane translational and the single in-plane rotational degrees of freedom.

where A is the wave amplitude, f is the number of ripples in a length $l_{cw}/2$, and x is the local coordinate between the initial and the final nodes of the wavy cell wall. For the Kagome and KT lattices, where all the cell walls have the same length, $f = 2$ is employed, while for the DK structures, $f = 2$ is used for the cell walls with $l_{cw1} = 0.4$ mm and $f = 4$ for $l_{cw2} = 0.8$ mm; see Section 2.2. The wave amplitude is taken to be $A = 0.05\ l_{cw}$ mm for the Kagome and KT lattices and $A = 0.05\ l_{cw1}$ for the DK lattice. Misaligned cell walls are inserted into the lattice block by displacing the nodes where cell walls meet. The vector $\boldsymbol{r}$ in Fig. 4d indicates the translation of one such node. Both the length and the direction of $\boldsymbol{r}$ are randomly assigned such that $l_{cws}/4 \le |r| \le l_{cws}/2$ and $0 \le \theta \le 2\pi$, where l_{cws} is the length of the shortest cell wall connected to the node and θ is the angle illustrated in Fig. 4d. Recall that cell walls with a non-uniform in-plane thickness are discretised with eight beam elements. The two beams at the two ends of the cell wall have the same thickness as the lattice's imperfection-free cell walls. The beam in-plane thickness decreases from the two ends towards the centre such that the thickness variation in the cell wall is symmetric with respect to its mid-point, see Fig. 4d. The thickness of a beam element located on either side of the mid-point is given by

$$t_k = \left(\frac{1-R}{3R}\right) t_{in} k - \left(\frac{1-4R}{3R}\right) t_{in}, \tag{3}$$

where t_k is the thickness of the element number $k = 1, 2, 3, 4$ and $R = 5$ is the in-plane thickness reduction ratio. Eq. (3) gives $t_1 = t_{in}$ for $k = 1$, and $t_4 = t_{in}/R = t_{in}/5 = t_{min}$ for $k = 4$, see Fig. 4(e).

The number of imperfections in the lattice block is dictated by f, which gives the percentage of the imperfect cell walls (respectively, the percentage of the displaced nodes for cell wall misalignment) with respect to the total number of cell walls (respectively, nodes) in the imperfection zone. The combined effect of different types of imperfections is examined by Grenestedt (2005) for closed-cell foams and Li et al. (2005) for Voronoi honeycombs, both showing very little interaction. They also found that the effects of different imperfections with small numbers were additive. Considering the results of Grenestedt (2005) and Li et al. (2005), the lattice block is allowed here to contain only a single type of imperfection at a time. Fig. 5 exemplifies the portions of the FE meshes for imperfect Kagome lattices containing (a) wavy cell walls, (b) misaligned cell walls, and (c) cell walls with a non-uniform thickness.

3. Results

The results of this study are presented below in two parts. In Section 3.1, a single imperfection is placed in the actuation corridor (along the cell walls aligned with the actuator as illustrated with a dashed line in Fig. 2, see also Fig. 7) while the remaining regions of the lattice block are imperfection-free. In Section 3.2, imperfections are randomly distributed within the imperfection zone. Unless otherwise stated, the results in the remainder are predicated on a relative density of $\bar{\rho} = 0.01$. This low relative density was chosen because the accuracy of the Euler–Bernoulli beam elements used in the FE models becomes questionable at higher relative densities, particularly for wavy cell walls and non-uniform thickness cell walls, which are discretised with 18 and 8 elements, respectively. Using beam elements is computationally much more efficient than using solid elements, but the downside of this choice is that slender beams corresponding to $\bar{\rho} = 0.01$ would be impractical to manufacture and prone to failure by buckling under macroscopic compressive loading. Nevertheless, Kagome lattices with $\bar{\rho} = 0.01$ and $\bar{\rho} = 0.1$ share the same tendencies for all calculations, as shown below, which justifies using $\bar{\rho} = 0.01$ for the two other (the DK and KT) lattices.

3.1. A single imperfection in the actuation corridor

Fig. 6 shows the distribution of the displacement magnitude, $U_{total} = \sqrt{U_1^2 + U_2^2}$, near the actuator in an imperfection-free Kagome lattice block with deformed by a single linear actuator located at the geometric centre of the block. The deformation of the lattice is confined to the actuation corridor with height $h_c \approx \sqrt{3}\, l_0$ (see Section 2.1), where Fig. 6 depicts a close-up view for clarity. U_{total} is most prominent at the tip of the actuator and decreases away from the tip. When the actuation corridor contains a single fractured cell wall or a single missing cell, the deformation immediately ceases where the imperfection is placed (see Figs. 7(a) and 7(b), respectively). The presence of one wavy (Fig. 7(c)) or misaligned (Fig. 7(d)) cell wall in the actuation corridor does not fully attenuate but reduces the deformation. The deformation is reduced to less than 20% and 60% of its initial value for the wavy and misaligned cell walls. A misaligned cell wall attenuates the deformation while generating an additional displacement field in a direction other than the horizontal infiltrating outside the actuation corridor. Among the five different imperfections, non-uniform cell wall thickness has the least significant effect on lattice deformation. As shown in Fig. 7(e), the cell wall with a non-uniform thickness itself deforms more than its imperfection-free neighbours, yet it can transmit the deformation wave without severely attenuating it.

The effects of an imperfection – fractured cell wall (FCW), missing cell (MC), cell wall waviness (CWW), cell wall misalignment (CWM), or non-uniform wall thickness (NUWT) – located in the actuation corridor of the Kagome lattice block on the normalised actuation energy, $\hat{W} = W/W_0$, and on the normalised attenuation distance, $\hat{l}_a = l_a/l_{a0}$, are

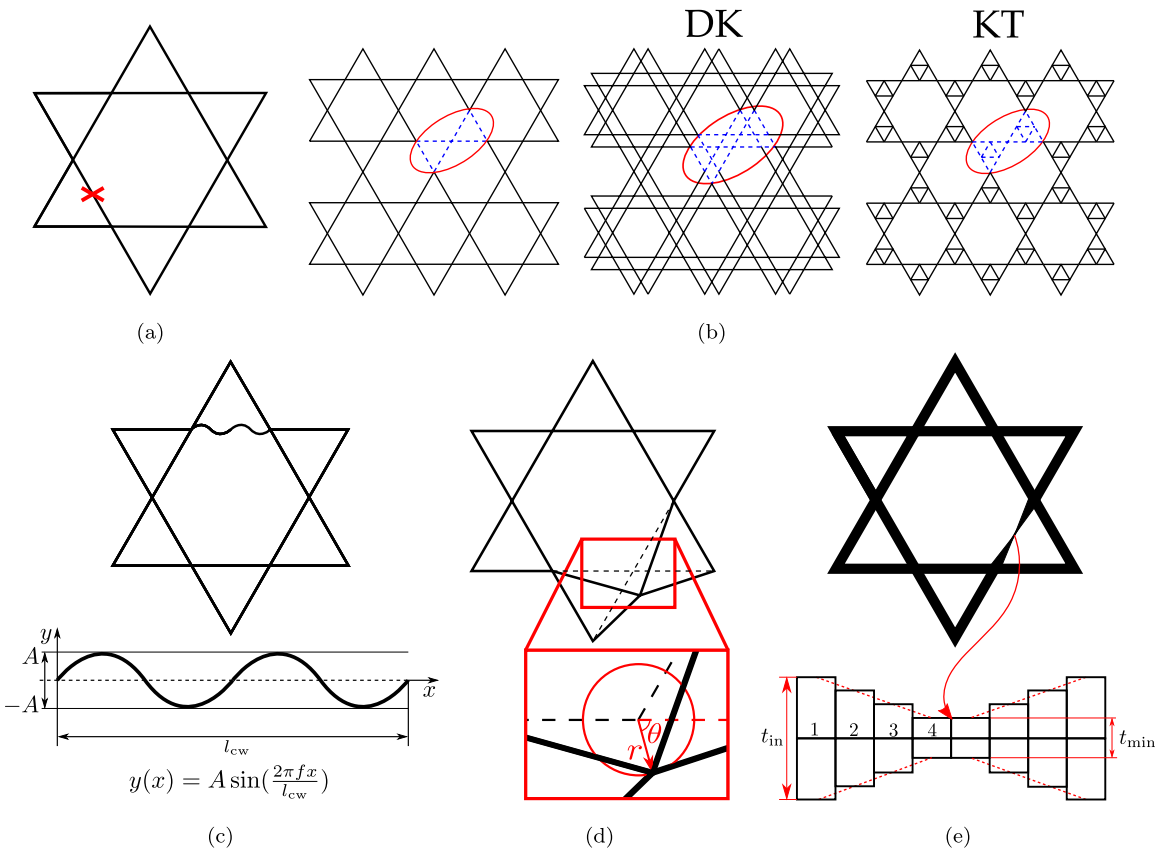

Fig. 4. Schematics showing the five different types of imperfections considered in this study: (a) fractured cell wall, (b) missing cell, (c) cell wall waviness, (d) cell wall misalignment, and (e) non-uniform cell wall thickness, see also Chen et al. (1999). The missing *cell* of the lattice is shown in (b) with encircled dashed lines for the Kagome, DK, and KT lattices.

given as functions of relative imperfection location, $l_{ri} = l_i/l_{a0}$, in Figs. 8(a) and 8(b), respectively. l_i denotes the distance between the imperfection and the nearest tip of the actuator, and l_{a0} and l_a are the attenuation distances in the perfect and imperfect Kagome blocks, respectively. We note in passing $l_i = 10$ mm and $l_{ri} = 0.06$ for Fig. 7.

As shown in Fig. 8(a), a fractured cell wall, missing cell, and cell wall waviness have similar effects on the actuation energy. The actuation energy is lowest for these three imperfections when the defect is closest to the actuator, i.e. for the smallest l_{ri} value. However, the corresponding low actuation energy does not indicate a better actuation performance here since it has been shown that FCW, MC, and CWW defects attenuate the displacement field very effectively. With increasing l_{ri}, actuation energy W increases and converges to W_0, albeit when $l_{ri} > 1$. The normalised actuation energy values are almost identical for a fractured cell wall and a missing cell for all l_{ri} values. At the same time, they are slightly larger for a wavy cell wall when $l_{ri} < 1$, because the local stiffness of the actuation corridor, which resists the deformation imposed by the actuator, decreases more due to a lacking cell wall or cell compared to a wavy cell wall. Another result revealed is that, although a cell wall with a non-uniform thickness deforms more than its imperfection-free neighbours, it does not affect the actuation energy. Unlike other imperfections, even a single joint can be misaligned in several ways due to the randomly selected $|r|$ and θ values (see Section 2.3). Therefore, Fig. 8 shows the average and the standard deviation (as error bars) of three different realisations for the cell wall misalignment imperfection. Depending on the new location of the displaced joint, the actuation energy can either increase or decrease for $l_{ri} < 1$, the standard deviation being considerably more prominent in the small l_{ri} regime. When any of the five imperfections is placed at a distance further than the attenuation distance of the perfect Kagome lattice, $W \to W_0$, i.e., for $l_{ri} \geq 1$, $\hat{W} \approx 1$. In fact, for a missing cell and a fractured cell wall, $\hat{W}$ is slightly below 1 for even beyond $l_{ri} = 1$.

The effects of a fractured cell wall, missing cell, and cell wall waviness on the normalised attenuation distance also share similar tendencies. For all three, the normalised attenuation distance coincides with the relative location of the defect, i.e., $\hat{l}_a = l_{ri}$ initially. This result can also be deduced from Fig. 7, where the displacement field induced by the actuator is instantly stopped by a fractured cell wall or a missing cell and considerably reduced by a wavy cell wall. The equality between $\hat{l}_a$ and l_{ri} extends beyond $l_{ri} = 1$, until $l_{ri} \approx 1.35$ for a fractured cell wall or a missing cell, and until $l_{ri} \approx 1.2$ for a wavy cell wall. In other words, by placing an imperfection beyond the attenuation distance of the perfect Kagome lattice, it is possible to increase its attenuation distance up to 35% if the defect is a fractured cell wall or a missing cell, and up to 20% if it is a wavy cell wall. The linear increase of $\hat{l}_a$ with increasing l_{ri} ceases once the peak value is reached, and l_a converges to l_{a0} for $l_{ri} > 2.5$ for all three imperfections. As in the case of actuation energy, non-uniform wall thickness does not affect the attenuation distance. The presence of misaligned cell walls tends to decrease the attenuation distance by an amount that depends on the $|r|$ and θ values in the regime $l_{ri} < 1$, but their effect is negligible for $l_{ri} > 1.5$.

The effects of an imperfection located in the actuation corridor of the Kagome lattice block as presented in Fig. 8 for $\bar{\rho} = 0.01$ is now given for $\bar{\rho} = 0.1$ in Fig. 9. By comparing Fig. 8 and Fig. 9, it can be deduced that the effect of normalised actuation energy and attenuation distance on relative fault location for $\bar{\rho} = 0.01$ and $\bar{\rho} = 0.1$ is qualitatively identical.

It remains to present the results for the DK and KT lattices depicted in Figs. 10 and 11, respectively. An essential difference between the three lattice micro-architectures considered is that the normalised attenuation distance in the perfect structure is $l_{a0}/l_0 = \{165, 96, 204\}$ respectively for the Kagome, DK, and KT micro-architectures. To highlight the differences in the actuation performance, the absolute distance

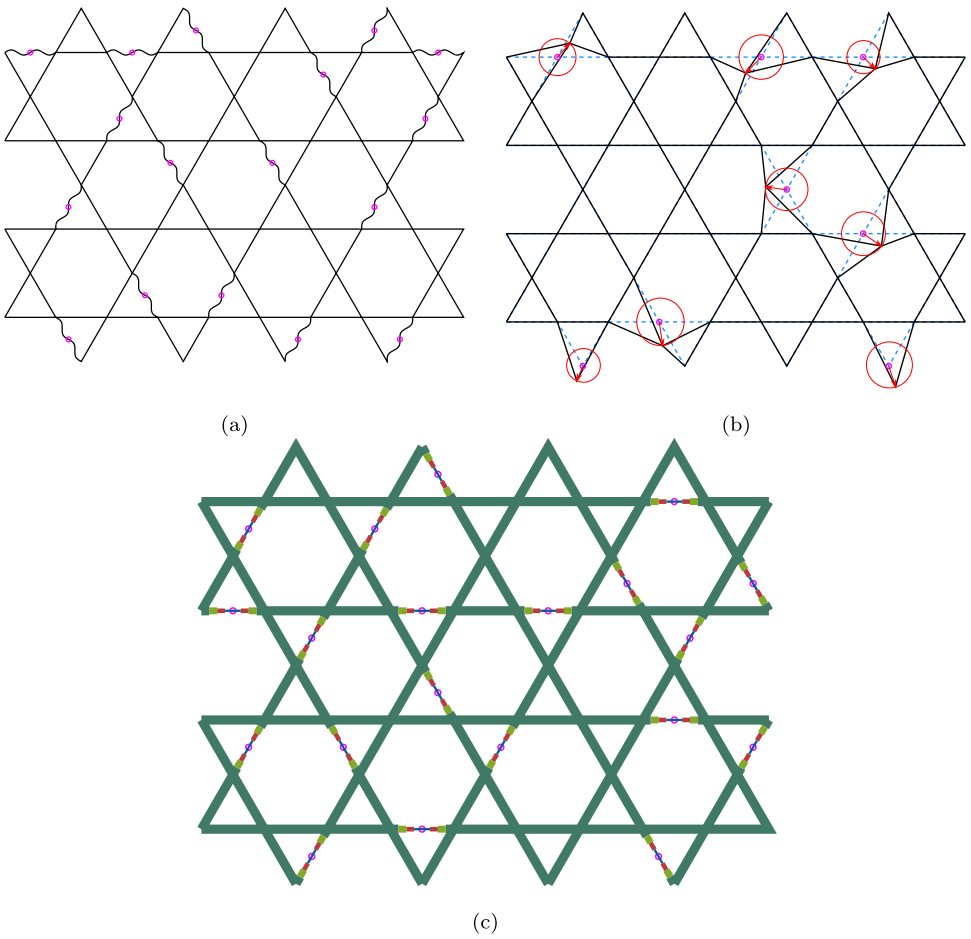

Fig. 5. FE mesh examples for the Kagome lattice with imperfections: (a) cell wall waviness, (b) cell wall misalignment, and (d) non-uniform cell wall thickness.

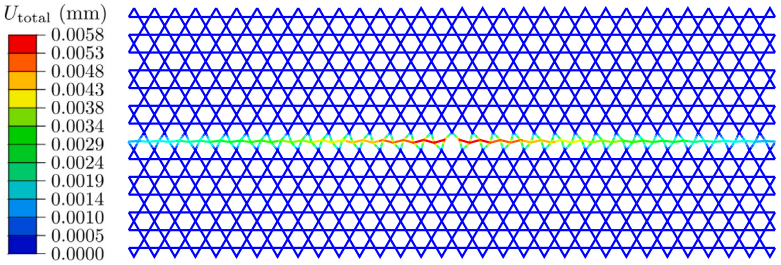

Fig. 6. Distribution of the total displacement, $U_{\text{total}} = \sqrt{U_1^2 + U_2^2}$, in an imperfection-free Kagome lattice block (with a relative density of $\bar{\rho} = 0.01$) deformed by a single linear actuator located at the geometric centre of the block. Deformations are amplified 50 times for the ease of visualisation.

of the imperfections from the actuator, l_{i}, is taken to be the same in all three lattices. Therefore, if the imperfection is, for example, at 165 mm away from the actuator, the corresponding $l_{\text{ri}} = \{1.00, 1.72, 0.81\}$ respectively for the Kagome, DK, and KT lattices. Accordingly, the ranges of x-axes differ in Figs. 8, 10, and 11, while the range of y-axes is kept the same for easy comparison. The effect of each type of imperfection shows the same trend in all three lattices, with some quantitative differences. Considering the normalised actuation energy for small l_{ri} values, the effects of a fractured cell wall and a missing cell are less severe for the DK lattice than the Kagome and KT lattices with a closer quantitative agreement. A wavy cell wall has the least significant effect on the KT lattice and the most significant on the Kagome lattice. For lattices containing misaligned cell walls, the largest value of $\hat{W}$ can go up to nearly 2.65 for the KT, 2.13 for the Kagome, and 1.42 for the DK lattice. The effect of imperfection on the attenuation distance correlates with its effect on the actuation energy. In the case of a fractured or a wavy cell wall or a missing cell, the normalised attenuation distance increase linearly with l_{ri} until it makes a peak beyond $l_{\text{ri}} > 1$, where it starts to decrease non-linearly to a value of $\hat{l}_{\text{a}} \approx 1$. The peak value of $\hat{l}_{\text{a}}$ is the largest for the missing cell defect (equal to that of a fractured cell wall defect for the Kagome and DK lattices) with $\hat{l}_{\text{a}} \approx 1.48$ for the KT, $\hat{l}_{\text{a}} \approx 1.35$ for the Kagome, and $\hat{l}_{\text{a}} \approx 1.26$ for the DK lattice. For the DK lattice, the effect of a wavy cell wall on the actuation performance depends on which of the two families of cell walls with different lengths contains the defect. If the wavy cell wall belongs to the family of short-length cell walls, the decrease in the attenuation distance is smaller, which can be observed from the $\hat{l}_{\text{a}}$ versus l_{ri} curve for CWW in Fig. 10(b). For the smallest value of l_{ri}, the imperfect cell wall happens to have a length of $l_{\text{cw}} = l_{\text{cw1}} = 0.4$ mm while for all other l_{ri} values, the wavy cell wall has the length $l_{\text{cw}} = l_{\text{cw2}} = 0.8$ mm, which explains the anomalous initial decrease in the $\hat{l}_{\text{a}}$ value. The decrease in the attenuation distance associated with cell wall misalignment is most

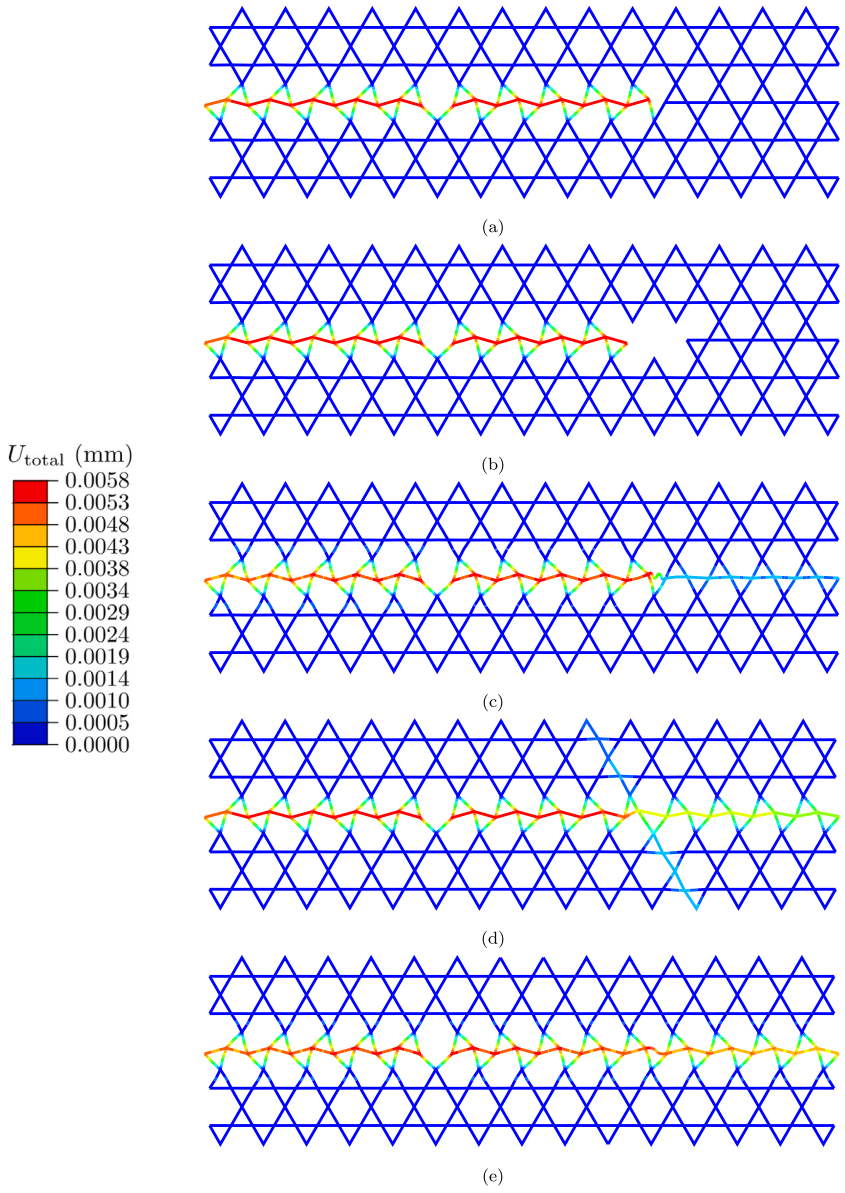

Fig. 7. Distribution of the total displacement, $U_{\text{total}} = \sqrt{U_1^2 + U_2^2}$, in an imperfect Kagome lattice block (with a relative density of $\bar{\rho} = 0.01$) deformed by a single linear actuator located at the geometric centre of the block. The lattice block contains a single (a) fractured cell wall, (b) missing cell, (c) wavy cell wall, (d) displaced joint (misaligning the cell walls connected to it), and (e) cell wall with a non-uniform thickness in the actuation corridor, and is otherwise imperfection free. All five imperfections are placed at the same distance from the tip of the actuator. Deformations are amplified 50 times for the ease of visualisation.

pronounced for the KT lattice, followed by the Kagome and DK lattices. Non-uniform cell wall thickness does not affect the actuation energy or the attenuation distance for these three lattice micro-architectures.

3.2. A random distribution of imperfections in the imperfection zone

In this section, $f = 1, 2, 5, 10\%$ imperfections are randomly distributed in the imperfection zone, while the actuation corridor and the close vicinity of the actuator are taken to be imperfection-free. Two different sets of analyses are performed: the imperfection zone's relative length (see Fig. 2) being $l/L = 1/8$ and $l/L = 1$. For each set, f represents the percentage of the imperfect cells, cell walls, or displaced joints relative to the corresponding total number in the imperfection zone, depending on the type of imperfection. The number of imperfections is eight times larger for $l/L = 1$ than for $l/L = 1/8$ for a fixed value of f.

Fig. 12 shows the distribution of the displacement magnitude, $U_{\text{total}} = \sqrt{U_1^2 + U_2^2}$, in a Kagome lattice block deformed by a single linear actuator located at its geometric centre. The block contains 10% fractured cell walls in Fig. 12a, missing cells in Fig. 12b, wavy cell walls in Fig. 12c, misaligned joints in Fig. 12d, and cell walls with a non-uniform in-plane thickness in Fig. 12e, randomly distributed in the imperfection zone with $l/L = 1/8$. For each type of imperfection, both the entire lattice block and the close-up view in the vicinity of the actuator are included in Fig. 12. For fractured cell walls and missing cells, the deformation emanating from the actuator spreads inside the imperfection zone, whereas it is confined to the actuation corridor in the imperfection-free parts of the block. For the other three imperfections, on the other hand, the deformation localises in the actuation corridor throughout the entire block.

Fig. 13 shows the effects of randomly distributed imperfections – fractured cell wall (FCW), missing cell (MC), cell wall waviness (CWW), cell wall misalignment (CWM), or non-uniform wall thickness (NUWT) – on the normalised macroscopic Young's modulus, $\hat{E} = E/E_0$, Figs. 13a and 13b, actuation energy, $\hat{W} = W/W_0$, Figs. 13c and 13d, and attenuation distance, $\hat{l}_a = l_a/l_{a0}$, Figs. 13e and 13f, as functions

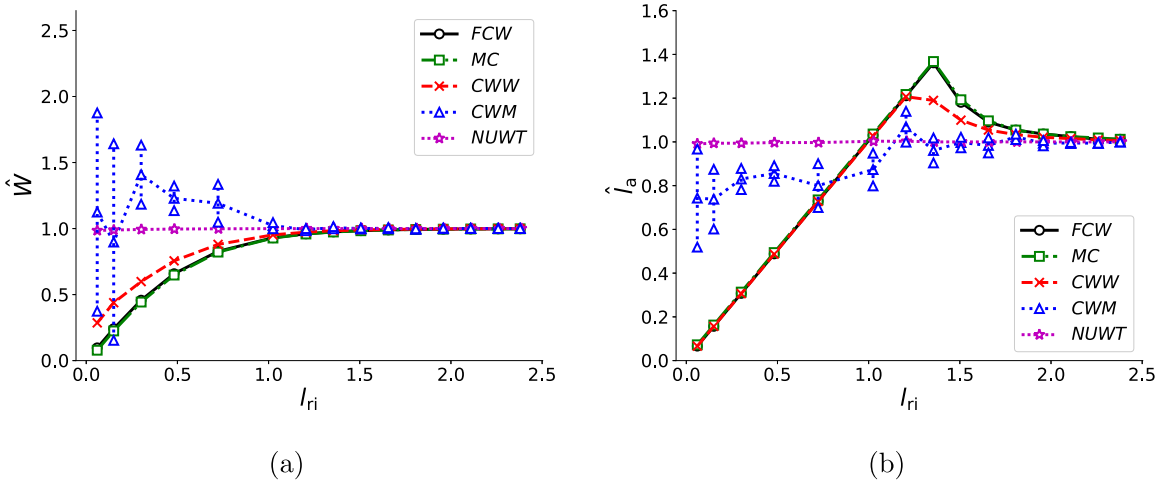

Fig. 8. Effect of an imperfection – fractured cell wall (FCW), missing cell (MC), cell wall waviness (CWW), cell wall misalignment (CWM), or non-uniform wall thickness (NUWT) – located in the actuation corridor of the Kagome lattice block (with a relative density of $\bar{\rho} = 0.01$) on the normalised (a) actuation energy, $\hat{W} = W/W_0$, and (b) attenuation distance, $\hat{l}_a = l_a/l_{a0}$, as a function of relative imperfection location, $l_{ri} = l_i/l_{a0}$. l_i denotes the distance of the imperfection from the closer tip of the actuator, and l_{a0} and l_a respectively the attenuation distances in the perfect and imperfect Kagome blocks.

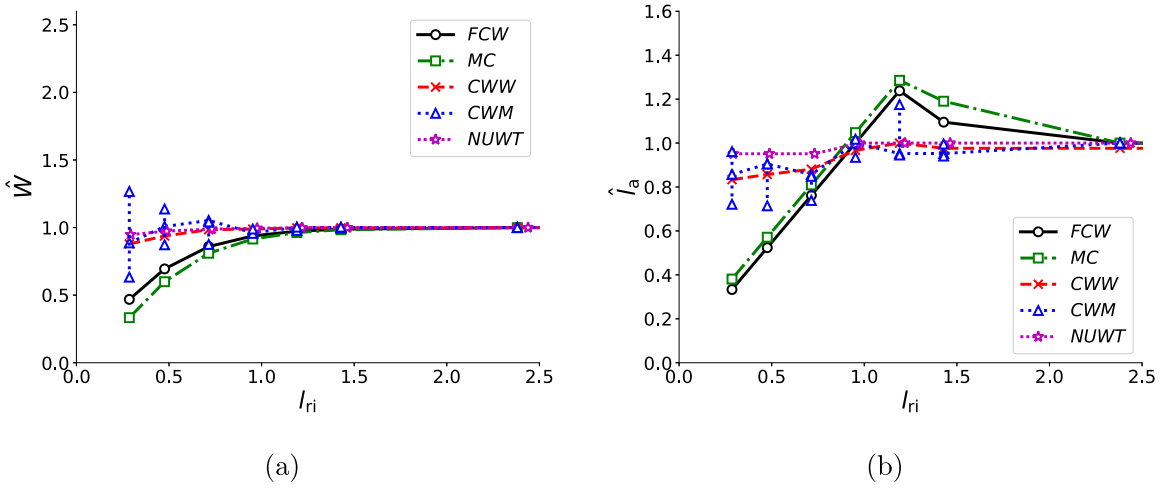

Fig. 9. Effect of an imperfection – fractured cell wall (FCW), missing cell (MC), cell wall waviness (CWW), cell wall misalignment (CWM), or non-uniform wall thickness (NUWT) – located in the actuation corridor of the Kagome lattice block (with a relative density of $\bar{\rho} = 0.1$) on the normalised (a) actuation energy, $\hat{W} = W/W_0$, and (b) attenuation distance, $\hat{l}_a = l_a/l_{a0}$, as a function of relative imperfection location, $l_{ri} = l_i/l_{a0}$.

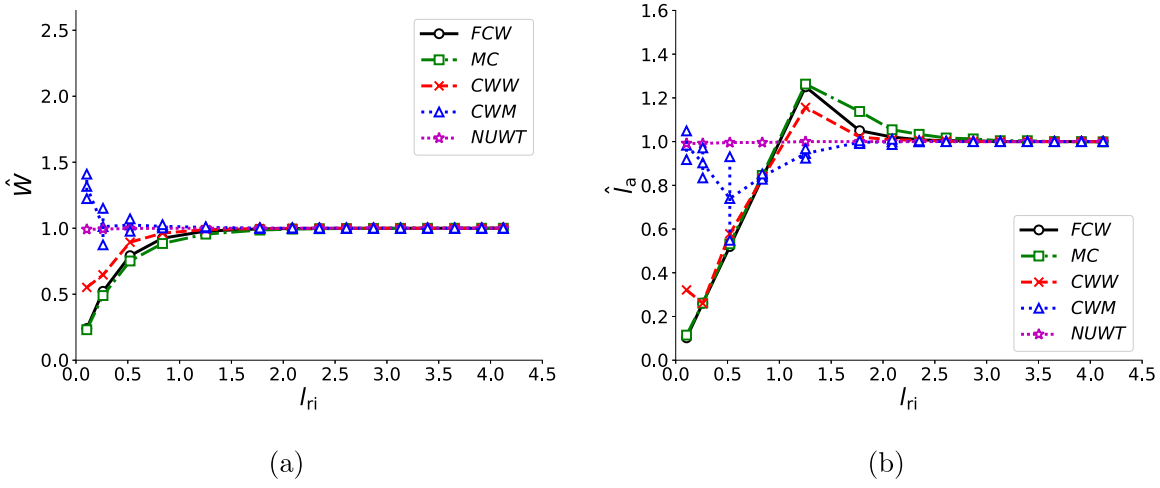

Fig. 10. Effect of an imperfection – fractured cell wall (FCW), missing cell (MC), cell wall waviness (CWW), cell wall misalignment (CWM), or non-uniform wall thickness (NUWT) – located in the actuation corridor of the DK lattice block (with a relative density of $\bar{\rho} = 0.01$) on the normalised (a) actuation energy, $\hat{W} = W/W_0$, and (b) attenuation distance, $\hat{l}_a = l_a/l_{a0}$, as a function of relative imperfection location, $l_{ri} = l_i/l_{a0}$.

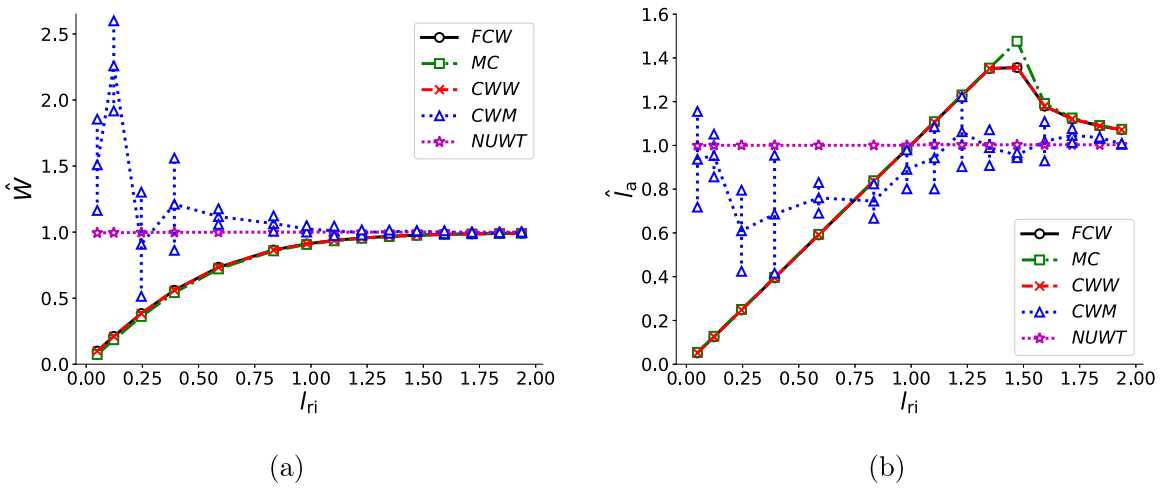

Fig. 11. Effect of an imperfection – fractured cell wall (FCW), missing cell (MC), cell wall waviness (CWW), cell wall misalignment (CWM), or non-uniform wall thickness (NUWT) – located in the actuation corridor of the KT lattice block (with a relative density of $\bar{\rho} = 0.01$) on the normalised (a) actuation energy, $\hat{W} = W/W_0$, and (b) attenuation distance, $\hat{l}_a = l_a/l_{a0}$, as a function of relative imperfection location, $l_{ri} = l_i/l_{a0}$.

of f for the Kagome lattice. The relative imperfection zone length is $l/L = 1/8$ in Figs. 13a, c and e, and $l/L = 1$ in Figs. 13b, d, and f. The normalised macroscopic Young's modulus, $\hat{E} = E/E_0$, denotes the ratio of the macroscopic Young's modulus of the imperfect (E) and perfect (E_0) blocks, obtained by performing uniaxial compression calculations, see Section 2.2. Six different realisations with random distributions of defects are analysed for each type of imperfection to account for the stochastic effect of the spatial distribution of the imperfections in the Kagome lattice. Fig. 13 presents the results with standard deviations as error bars.[3] All types of imperfection cause a knock-down in $\hat{E}$ with increasing f. In descending order, the greatest knock-down occurs for fractured cell walls, followed by missing cells, wavy cell walls, misaligned cell walls, and cell walls with a non-uniform wall thickness. The level of knock-down is comparable for the fractured cell walls, missing cells, and wavy cell walls, but significantly less for non-uniform wall thickness, and assumes intermediate values for misaligned cell walls. $\hat{E}$ decreases non-linearly for all types of imperfection, except for non-uniform wall thickness, where it follows a linear trend. For an imperfection zone with $l/L = 1/8$ and $f = 10\%$, $\hat{E} \approx 0.8$ for fractured cell walls, while $\hat{E} \approx 0.98$ for non-uniform wall thickness (Fig. 13a). Except for non-uniform wall thickness, the knock-down effect is significantly more pronounced when $l/L = 1$: even for $f = 1\%$, $\hat{E} \approx 0.22$ for fractured cell walls, $\hat{E} \approx 0.33$ for missing cells, $\hat{E} \approx 0.39$ for wavy cell walls, and $\hat{E} \approx 0.75$ for misaligned cell walls; for $f = 10\%$, $\hat{E}$ is nearly zero for fractured cell walls and missing cells (Fig. 13b). Considering the normalised actuation energy, $\hat{W} = W/W_0$, the ordering of the knock-down levels remains the same as in $\hat{E}$, except that the reduction is slightly more pronounced for non-uniform wall thickness than for misaligned cell walls in this case (Figs. 13c, d). $\hat{W}$ is practically insensitive to misaligned cell walls, but it is considerably reduced due to fractured cell walls and missing cells. The knock-down in $\hat{W}$ increases with increasing f. The normalised attenuation distance, $\hat{l}_a$, increases with increasing f for fractured or wavy cell walls and missing cells. Fractured cell walls cause the highest rate of increase and wavy cell walls the lowest. Non-uniform wall thickness has no effect on $\hat{l}_a$, and the effect of cell wall misalignment is marginal; it can only slightly decrease or increase $\hat{l}_a$, depending on the spatial distribution of the displaced joints. The effect of each type of imperfection follows the same trend for $l/L = 1/8$ and $l/L = 1$, the difference being that the knock-down or increase in a parameter of interest is larger for $l/L = 1$.

[3] Since the standard deviation of the results for the Kagome block came out to be rather small, the number of different random realisations are limited to three for the DK and KT lattices; see Figs. 15 and 16

In order to see the effect of member thickness on the trends discussed above, the effect of randomly distributed imperfections on the normalised macroscopic Young's modulus, $\hat{E} = E/E_0$, actuation energy, $\hat{W} = W/W_0$, and attenuation distance, $\hat{l}_a = l_a/l_{a0}$ is investigated for $\bar{\rho} = 0.1$ and the results are given in Fig. 14. Upon comparing Fig. 14 with Fig. 13, it is evident that the effect of all kinds of imperfections on Young's modulus, actuation energy and attenuation distance are qualitatively identical.

Figs. 15 and 16 show the companion results for the DK and KT lattices, plotted on the same ranges of $x-$ and $y-$axes as the Kagome lattice for easy comparison. Again, the imperfection sensitivity of the macroscopic Young's modulus, actuation energy, and attenuation distance for all three lattices evolve in the same way with increasing f, the main difference being in the actual values.

The level of knock-down in the normalised macroscopic Young's modulus due to non-uniform wall thickness is almost the same in the three lattices. The KT lattice is the least sensitive to misaligned cell walls, and the Kagome lattice is the most. The knock-down for the DK lattice is slightly less than the Kagome lattice. The knock-down due to fractured cell walls, missing cells, and cell wall waviness, listed in descending order, is most pronounced for the KT lattice. The Kagome and DK lattices are equally sensitive to missing cells and cell wall waviness, but the reduction rate with increasing f in the normalised macroscopic Young's modulus associated with fractured cell walls is more prominent in the DK lattice than in the Kagome lattice, especially when $f < 5\%$.

Regarding the normalised actuation energy, all three lattices are insensitive to cell wall misalignment and only marginally sensitive to non-uniform wall thickness. The greatest knock-down in $\hat{W}$ occurs for fractured cell walls in each lattice, followed by missing cells and wavy cell walls in descending order. The level of knock-down due to fractured cell walls and missing cells is the greatest for the KT lattice and the smallest for the DK lattice. The effect of cell wall waviness, on the other hand, is most pronounced for the Kagome lattice while affecting the DK slightly less than for the KT lattice.

Similar to the case of the actuation energy, cell wall misalignment and non-uniform wall thickness have negligible effects on the attenuation distance. However, fractured cell walls, missing cells, and wavy cell walls cause an increase in the normalised attenuation distance in all the three lattice micro-architectures, the magnitude of increase descending in the given order. The DK lattice is the most sensitive to fractured cell walls and missing cells, and the Kagome lattice to cell wall waviness.

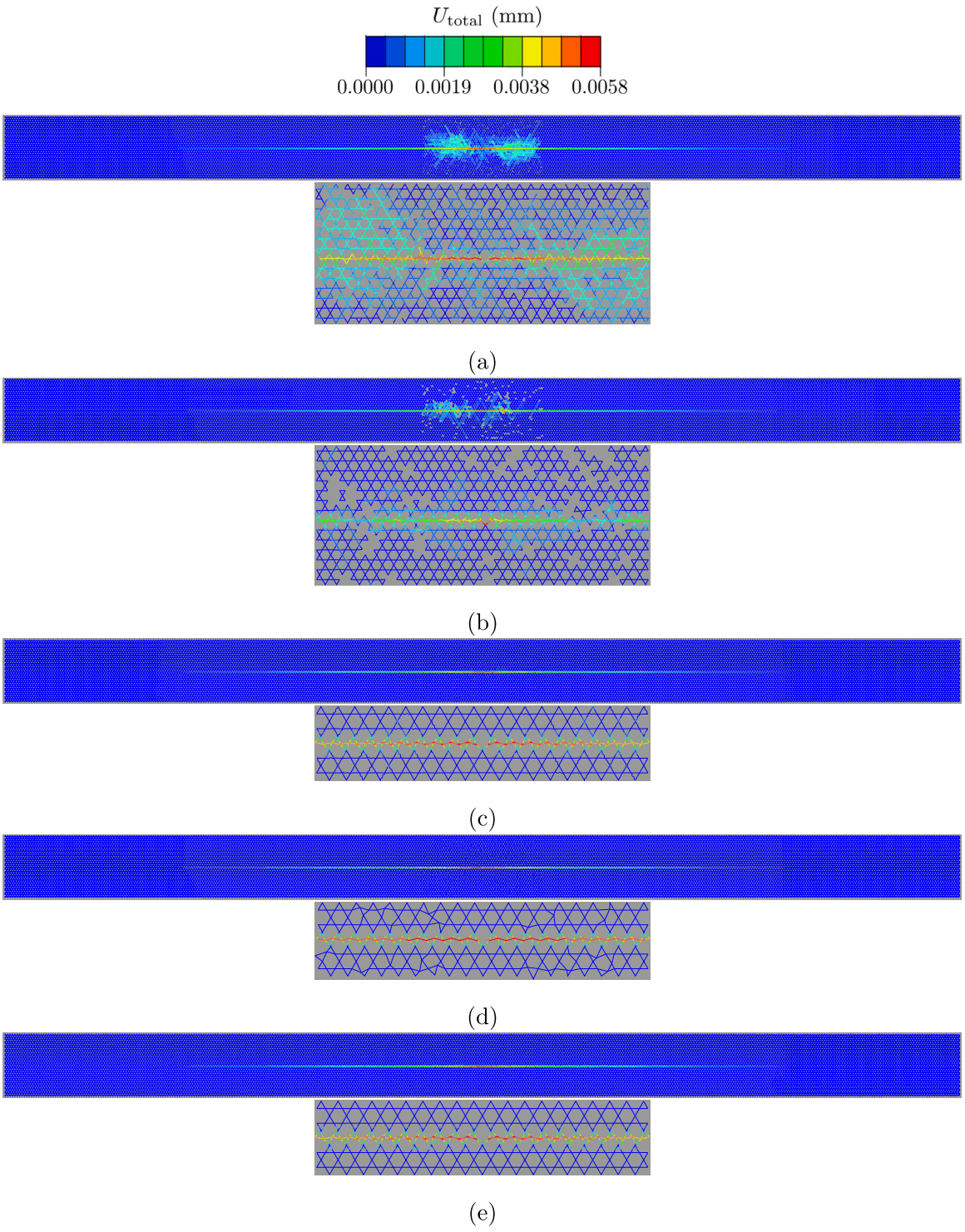

Fig. 12. Distribution of the total displacement, $U_{\text{total}} = \sqrt{U_1^2 + U_2^2}$, in a Kagome lattice block (with a relative density of $\bar{\rho} = 0.01$) deformed by a single linear actuator located at the geometric centre of the block. The block contains 10% (a) fractured cell walls, (b) missing cells, (c) wavy cell walls, (d) misaligned joints, and (e) cell walls with a non-uniform in-plane thickness, randomly distributed in the imperfection zone having a relative length of $l/L = 1/8$, see Fig. 2. For each type of imperfection, the top figure shows the entire lattice block and the bottom figure the close vicinity of the actuator. Deformations are amplified 50 times for the ease of visualisation.

4. Discussion

Recall that an ideal lattice material for actuation has a stiff, stretching-dominated and isotropic elastic response in the absence of actuation combined with a compliant and bending-dominated elastic response during actuation. Also, the deformation mode of a lattice material, i.e., stretching- or bending-dominated, can be traced back to the rigidity of the equivalent repetitive pin-jointed truss (Deshpande et al., 2001). In short, statically determinate micro-architectures satisfying the Maxwell–Calladine criterion are suitable for actuation, granted exhibiting only non-strain-producing mechanisms.

Nelissen et al. (2019) determined the number of self-stress states s and the number of inextensional mechanisms m of the KT repetitive trusses as $s = m = 3$ (which is identical to that Kagome truss (Guest and Hutchinson, 2003)), and the DK repetitive truss as $s = m = 6$. Two of the

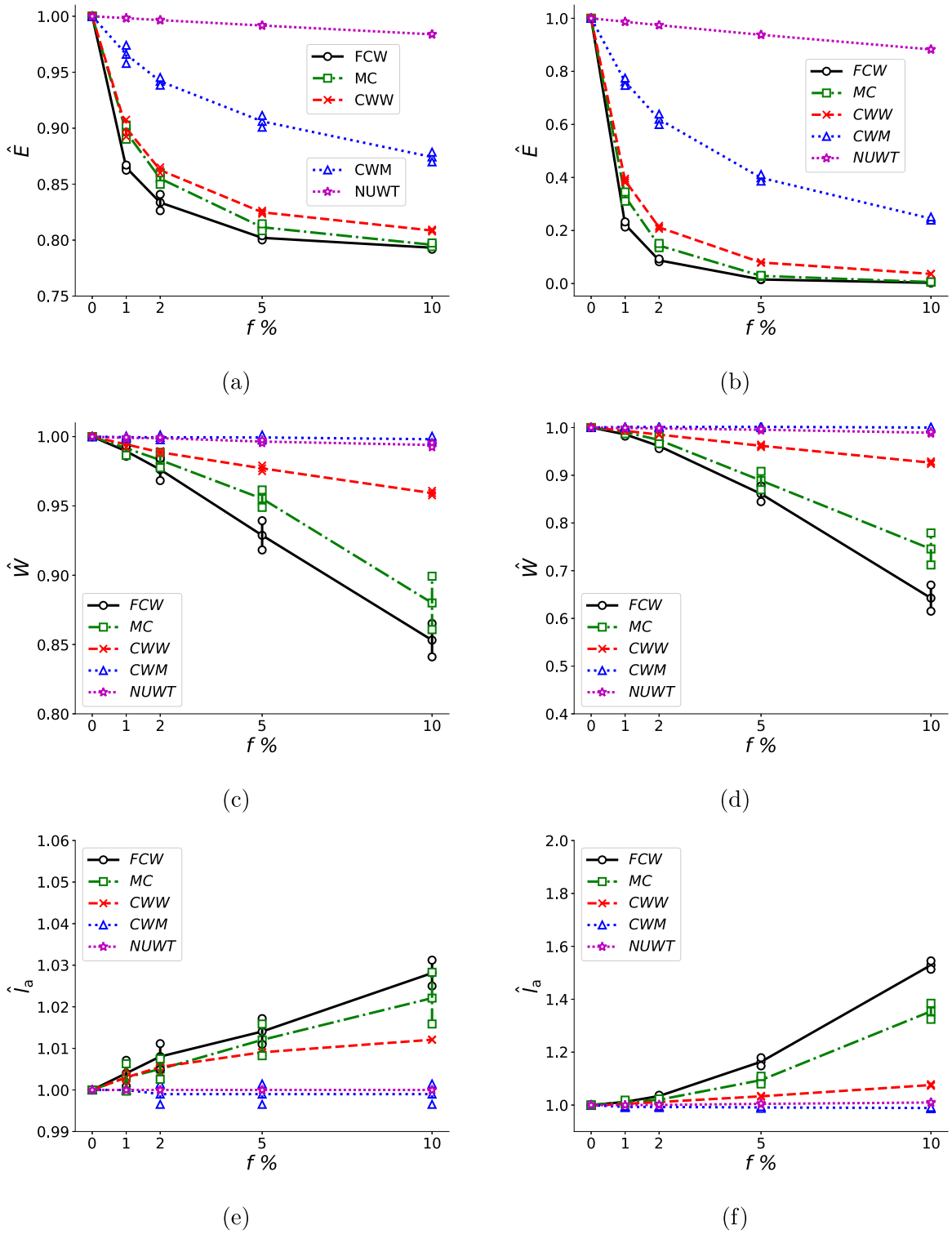

Fig. 13. Effect of randomly distributed imperfections – fractured cell wall (FCW), missing cell (MC), cell wall waviness (CWW), cell wall misalignment (CWM), or non-uniform wall thickness (NUWT) – in the imperfection zone of the Kagome lattice block (with a relative density of $\bar{\rho} = 0.01$) on the normalised (a, b) effective stiffness, $\hat{E} = E/E_0$, (c, d) actuation energy, $\hat{W} = W/W_0$, and (e, f) attenuation distance, $\hat{l}_a = l_a/l_{a0}$, as a function of imperfection percentage, f. The relative imperfection zone length is $l/L = 1/8$ in (a, c, e), and $l/L = 1$ in (b, d, f), see Fig. 2.

total inextensional mechanisms in all repetitive trusses are rigid body translations in x_1 and x_2 directions. Note that all three planar micro-architectures of interest are isotropic and satisfy the Maxwell–Calladine criterion with a coordination number of $Z = 4$. The three possible macroscopic stress states in 2D are sustained for each repetitive truss through linear combinations of the states of self-stress they possess. Therefore, all three trusses are "just rigid" and have only non-strain-producing collapse mechanism(s). The Kagome and KT trusses each have one non-strain-producing collapse mechanism, whereas the DK truss has four.

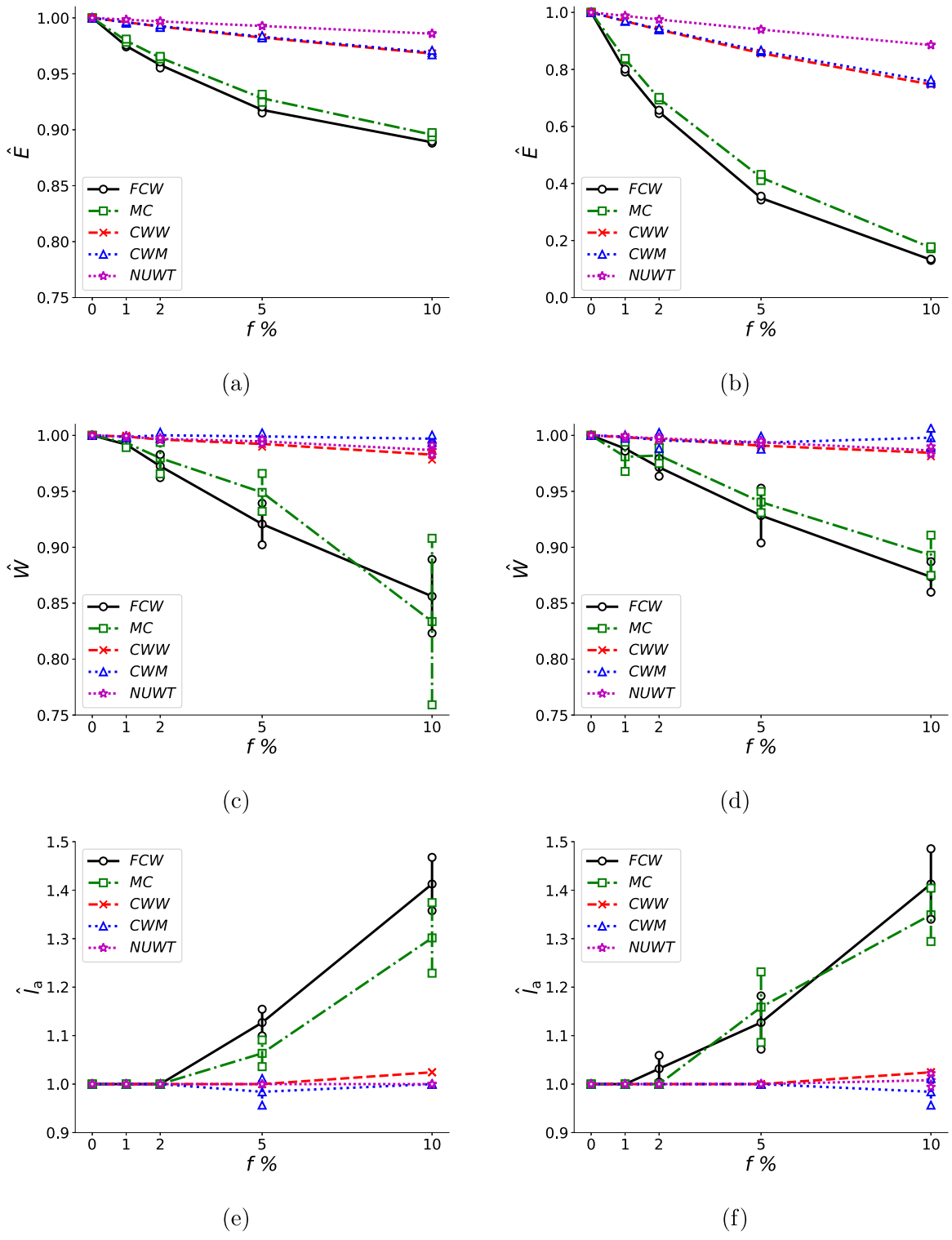

Fig. 14. Effect of randomly distributed imperfections – fractured cell wall (FCW), missing cell (MC), cell wall waviness (CWW), cell wall misalignment (CWM), or non-uniform wall thickness (NUWT) – in the imperfection zone of the Kagome lattice block (with a relative density of $\bar{\rho} = 0.1$) on the normalised (a, b) effective stiffness, $\hat{E} = E/E_0$, (c, d) actuation energy, $\hat{W} = W/W_0$, and (e, f) attenuation distance, $\hat{l}_a = l_a/l_{a0}$, as a function of imperfection percentage, f. The relative imperfection zone length is $l/L = 1/8$ in (a, c, e), and $l/L = 1$ in (b, d, f), see Fig. 2. $\bar{\rho} = 0.1$.

The non-strain-producing collapse mechanism for the KT truss is shown in Fig. 17 as an example. This mechanism consists of unit cell periodic rotation of alternating triangles in opposite directions. Although any uniform macroscopic loading cannot trigger this non-strain producing mechanism, forces associated with the actuation can induce rotation of alternating triangles in a KT truss upon replacing a member with an actuator. The corresponding rigid jointed KT lattice material thus exhibits a bending-dominated compliant deformation during actuation, c.f. Figs. 1c and 17. Consequently allowing for a considerable attenuation distance and low actuation energy. Similar excitation of non-strain-producing mechanisms occurs with actuation

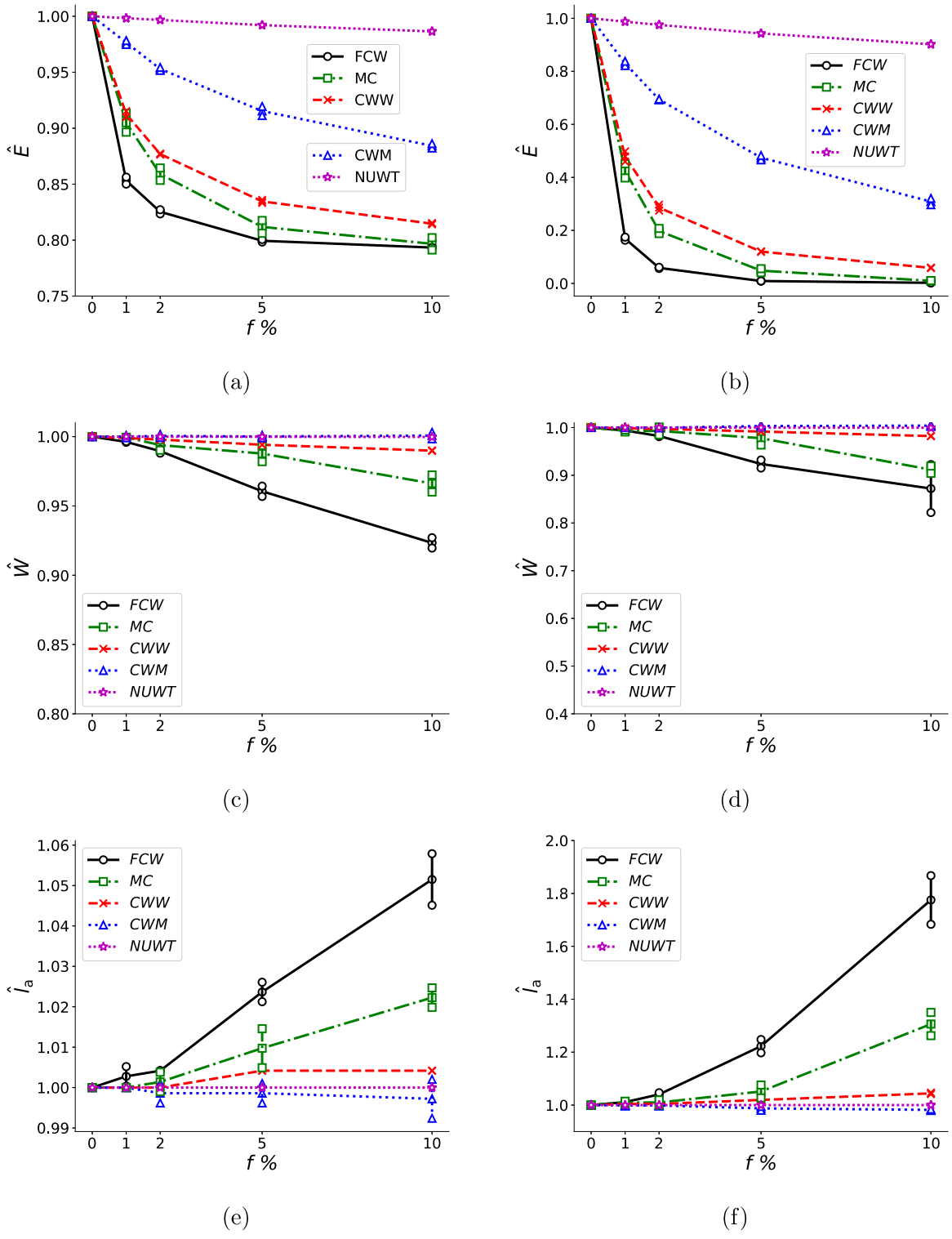

Fig. 15. Effect of randomly distributed imperfections – fractured cell wall (FCW), missing cell (MC), cell wall waviness (CWW), cell wall misalignment (CWM), or non-uniform wall thickness (NUWT) – in the imperfection zone of the DK lattice block (with a relative density of $\bar{\rho} = 0.01$) on the normalised (a, b) effective stiffness, $\hat{E} = E/E_0$, (c, d) actuation energy, $\hat{W} = W/W_0$, and (e, f) attenuation distance, $\hat{l}_a = l_a/l_{a0}$, as a function of imperfection percentage, f. The relative imperfection zone length is $l/L = 1/8$ in (a, c, e), and $l/L = 1$ in (b, d, f), see Fig. 2.

in DK and Kagome trusses, implying bending-dominated compliant deformation during actuation in these micro-architectures.

The macroscopic Young's modulus ($\hat{E}$) and actuation energy ($\hat{W}$) for a lattice depend on how compliant the lattice is during actuation with the inclusion of the imperfections. All three lattice micro-architectures of interest have exhibited a high sensitivity to the presence of imperfections in $\hat{E}$ and $\hat{W}$. This is anticipated for the micro-architectures that are "just rigid" in the pin-jointed truss form satisfying the Maxwell–Calladine condition with $s = m$ or $Z = 4$. Since, in "just rigid" micro-architectures, the deformation mode switches from axial to bending

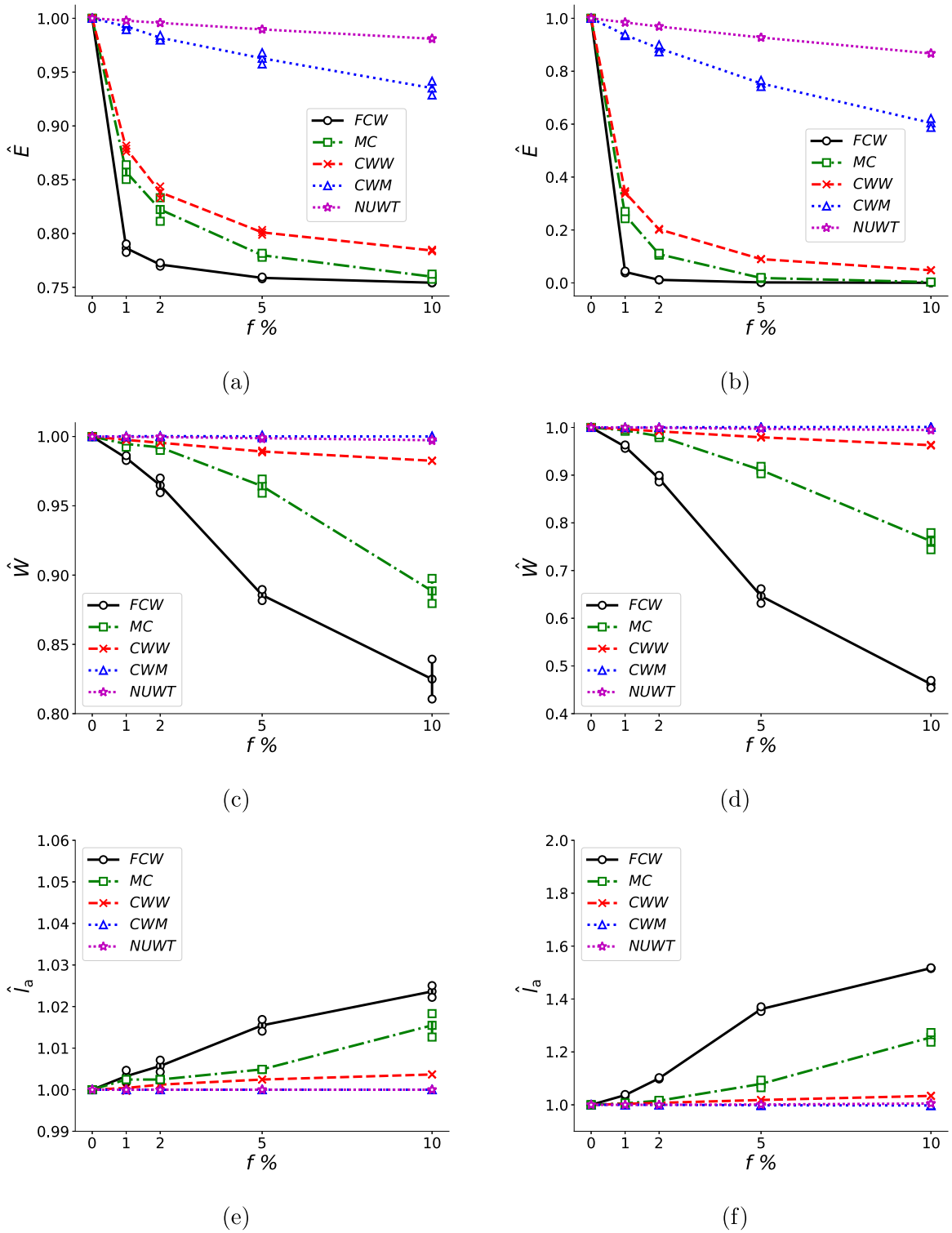

Fig. 16. Effect of randomly distributed imperfections – fractured cell wall (FCW), missing cell (MC), cell wall waviness (CWW), cell wall misalignment (CWM), or non-uniform wall thickness (NUWT) – in the imperfection zone of the KT lattice block (with a relative density of $\bar{\rho} = 0.01$) on the normalised (a, b) effective stiffness, $\hat{E} = E/E_0$, (c, d) actuation energy, $\hat{W} = W/W_0$, and (e, f) attenuation distance, $\hat{l}_a = l_a/l_{a0}$, as a function of imperfection percentage, f. The relative imperfection zone length is $l/L = 1/8$ in (a, c, e), and $l/L = 1$ in (b, d, f), see Fig. 2.

due to the presence of imperfections. On the other hand, Symons and Fleck (2008) showed that lattice micro-architectures that are kinematically indeterminate or statically redundant are relatively insensitive to imperfections. This is rationalised since elastic deformation of lattice material composed of the former micro-architecture is typically bending-dominated while the latter is typically stretching-dominated, irrespective of imperfections.

The knock-down in the macroscopic Young's modulus of the Kagome, DK, and KT lattices is most significant for fractured cell walls, followed by missing cells, cell wall waviness, cell wall misalignment, and non-uniform cell wall thickness in descending order. Fractured cell

walls decrease the lattice's connectivity (the coordination number Z), inducing kinematic indeterminacy of the equivalent pin-jointed truss. This explains the substantial reduction of macroscopic Young's modulus through increasing the degree of bending in the rigid jointed lattice material. Missing cells are clusters of fractured cell walls. Clustering renders the effect of fractured cell walls more localised, i.e., the coordination numbers Z of remaining members are less affected than the same number of scattered missing cells, which rationalises the diminishing degree of overall macroscopic Young's modulus reduction. Similar to fractured cell walls and missing cells, wavy cell walls also cancel out the kinematic determinacy of the equivalent pin-jointed truss. Therefore, the knock-down levels due to fractured cell walls, missing cells, and cell wall waviness are comparable. Cell wall misalignment exhibits a smaller effect. This imperfection does not cause a violation of the Maxwell–Calladine condition for the equivalent pin-jointed truss, yet it changes the local static/kinematic determinacy in the finite region containing the imperfection. This highlights that the Maxwell–Calladine condition is necessary but not sufficient for rigidity. Non-uniform wall thickness, which slightly changes the axial and bending stiffness of the imperfect struts, marginally reduces the macroscopic Young's modulus since the static/kinematic determinacy of the equivalent pin-jointed truss is conserved. Moreover, struts in line with the actuator deform in double bending so that the mid-point of each member is a point of contra-flexure. The reduction of wall thickness at the middle of a bar will therefore have very little effect on the stiffness.

The degree of knock-down in the macroscopic Young's modulus is correlated by a corresponding reduction in the actuation energy for fractured, wavy, or non-uniform cell walls and missing cells. In contrast, cell wall misalignment barely affects the actuation energy, which can be explained as follows. The actuation energy is spent mainly to deform the lattice members located in the actuation corridor (and partially to the scattering of the displacement field due to imperfections). Therefore, the critical parameter that defines the actuation energy is the stiffness along the actuation corridor. Misaligned cell walls only affect the close neighbourhood of the defect and have a negligible effect on the actuation energy when located outside the actuation corridor. Comparing the evolution of actuation energy and attenuation distance with the increasing number of imperfections reveals that the lower the stiffness along the actuation corridor, the longer the attenuation distance and the lower the actuation energy. Nevertheless, since the attenuation distance increases at the expense of the macroscopic Young's modulus, the lattice becomes more prone to failure and is not useful for shape morphing applications.

The displacement field induced by an actuator in the three microarchitectures immediately ceases when encountering a fractured cell wall or a missing cell since a displacement field needs a medium to propagate. The presence of a wavy cell wall in the actuation corridor is comparable to that of a fractured cell wall or missing cell in that the displacement magnitude reduces to less than 20% of its initial value passing through a wavy wall. This significant reduction in the displacement magnitude is that a substantial fraction of the actuation energy provided to the system is stored in the wavy cell wall, which deforms almost entirely by bending. A cell wall with a non-uniform thickness in the actuation corridor, on the other hand, has no effect on the actuation energy or attenuation distance, despite deforming more than its defect-free neighbours, because the thickness of the cell wall reaches its minimum value at the cell wall's mid-point, which is the point of contra-flexure. Unlike the other four types of imperfection, a misaligned joint can either increase or decrease the actuation energy and the attenuation distance depending on the new location of the joint. Moving far away from the actuator, the effects of all five imperfections die out. A significant result revealed by this study is that a fractured or wavy cell wall or a missing cell located in the actuation corridor might increase the attenuation distance while preserving the macroscopic Young's modulus of the lattice. This is attained when the defect is placed just far enough from the actuator, i.e., beyond the attenuation distance of the perfect lattice, but close enough that the actuator can still feel the reduction in stiffness.

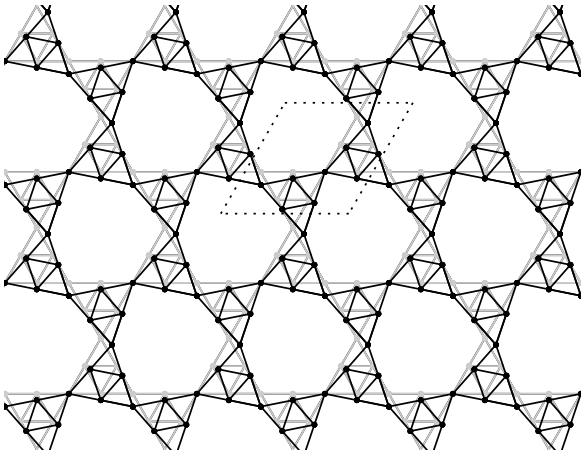

Fig. 17. Linearised representations of the unit cell periodic mechanisms of the repetitive KT truss, see also Nelissen et al. (2019).

5. Conclusions

The effects of five different types of imperfections – fractured cell walls, missing cells, cell wall waviness, cell wall misalignment and non-uniform wall thickness – on the macroscopic Young's modulus and actuation performance are numerically explored for the Kagome, DK, and KT latices. The lattice block is excited by a single linear actuator located at its centre, and either a single imperfection is placed in the actuation corridor, or imperfections are randomly distributed in the imperfection zone outside the actuation corridor. The key findings of this study are listed below.

- The actuation energy and the attenuation distance for the lattice mainly depend on the stiffness along the actuation corridor: the less stiff the corridor is, the lower the actuation energy and the higher the attenuation distance.
- Suppose the actuation corridor contains a fractured or wavy cell wall or a missing cell located at a distance from the actuator less than the attenuation distance in the perfect lattice. In that case, the deformation imposed by the actuator attenuates precisely on the defect. On the other hand, if the defect is located slightly beyond the attenuation distance in the perfect lattice, it increases the attenuation distance in the imperfect lattice: a defect intentionally placed as a design feature at a "correct" position might be beneficial for shape morphing applications.
- A cell wall with a non-uniform thickness in the actuation corridor does not affect the actuation performance. However, depending on the new location of the displaced joint, misaligned cell walls in the actuation corridor can either increase or decrease the actuation energy and decrease the attenuation distance. None of the five defects does affect the actuation performance when sitting alone in the actuation corridor, sufficiently removed from the actuator.
- The presence of randomly distributed imperfections in the imperfection zone outside the actuation corridor degrades the macroscopic Young's modulus of the lattice. The reduction in the actuation performance associated with the knock-down in the macroscopic Young's modulus depends on the type of imperfection. The effect of a misaligned joint, for example, spreads only to its close vicinity, and therefore even 10% of misaligned joints in the imperfection zone do not affect the actuation performance of the lattice. However, randomly distributed imperfections make the lattice more prone to failure and less useful for shape morphing applications.

- Both the actuation performance and the imperfection tolerance of the DK and KT lattices are comparable to those of the Kagome lattice. Therefore, these two lattices seem good alternatives for the Kagome lattice in shape morphing applications.

Declaration of competing interest

The authors declare that they have no known competing financial interests or personal relationships that could have appeared to influence the work reported in this paper.

Acknowledgements

The authors gratefully acknowledge the financial support by TÜBİTAK (The Scientific and Technological Research Council of Turkey, Project Title: Design of New Multi-Functional Lattice Materials; Project No: 219M296).

References

Abaqus, 2020. Abaqus documentation collection. Version 2020, Providence. Dassault Systèmes.

Ayas, C., Tekoğlu, C., 2018. On the sufficient symmetry conditions for isotropy of elastic moduli. J. Appl. Mech. 85, 074502. http://dx.doi.org/10.1115/1.4039952.

Bornengo, D., Scarpa, F., Remillat, C., 2005. Evaluation of hexagonal chiral structure for morphing airfoil concept. Proc. Inst. Mech. Eng. G 219, 185–192. http://dx.doi.org/10.1243/095441005X30216.

Calladine, C., 1978. Buckminster fuller's tensegrity structures and Clerk Maxwell's rules for the construction of stiff frames. Int. J. Solids Struct. 14, 161–172. http://dx.doi.org/10.1016/0020-7683(78)90052-5.

Chen, C., Lu, T., Fleck, N., 1999. Effect of imperfections on the yielding of two-dimensional foams. J. Mech. Phys. Solids 47, 2235–2272. http://dx.doi.org/10.1016/S0022-5096(99)00030-7.

Cheung, K., Cellucci, D., Copplestone, G., Cramer, N., Fusco, J., Jenett, B., Kim, J., Langford, A., Mazhari, A., Trinh, G., Clinkaberry, T., Formoso, O., Swei, S.S.M., 2017. Development of mission adaptive digital composite aerostructure technologies (MADCAT). http://arxiv.org/abs/https://arc.aiaa.org/doi/pdf/10.2514/6.2017-4273.

Cuadrado, A., Yánez, A., Martel, O., Deviaene, S., Monopoli, D., 2017. Influence of load orientation and of types of loads on the mechanical properties of porous ti6al4v biomaterials. Mater. Des. 135, 309–318. http://dx.doi.org/10.1016/j.matdes.2017.09.045.

Daynes, S., Weaver, P.M., 2013. Review of shape-morphing automobile structures: Concepts and outlook. Proc. Inst. Mech. Eng. D 227, 1603–1622. http://dx.doi.org/10.1177/0954407013496557.

De-Nicola, F., Totaro, G., Giusto, G., Spena, P., Kiryenko, S., Das, S., 2021. An efficient and scalable manufacturing method for CFRP lattice structures for satellite central tube and large deployable antenna boom applications. CEAS Space J. http://dx.doi.org/10.1007/s12567-021-00391-3.

Deshpande, V., Ashby, M., Fleck, N., 2001. Foam topology: Bending versus stretching dominated architectures. Acta Mater. 49, 1035–1040. http://dx.doi.org/10.1016/S1359-6454(00)00379-7.

Donev, A., Torquato, S., 2003. Energy-efficient actuation in infinite lattice structures. J. Mech. Phys. Solids 51, 1459–1475. http://dx.doi.org/10.1016/S0022-5096(03)00048-6.

dos Santos e Lucato, S., Wang, J., Maxwell, P., McMeeking, R., Evans, A., 2004. Design and demonstration of a high authority shape morphing structure. Int. J. Solids Struct. 41, 3521–3543. http://dx.doi.org/10.1016/j.ijsolstr.2004.02.012.

Echeta, I., Feng, X., Dutton, B., Leach, R., Piano, S., 2020. Review of defects in lattice structures manufactured by powder bed fusion. Int. J. Adv. Manuf. Technol. 106, 2649–2668. http://dx.doi.org/10.1007/s00170-019-04753-4.

Fleck, N., Deshpande, V., Ashby, M., 2010. Micro-architectured materials: Past, present and future. Proc. Royal Soc. A 466, 2495–2516. http://dx.doi.org/10.1098/rspa.2010.0215.

Galy, C., Guen, E.Le., Lacoste, E., Arvieu, C., 2018. Main defects observed in aluminum alloy parts produced by SLM:From causes to consequences. Addit. Manuf. 22 (165), http://dx.doi.org/10.1016/j.addma.2018.05.005.

Gibson, I., Rosen, D.W., Stucker, B., Khorasani, M., 2021. Additive Manufacturing Technologies. Vol. 17. Springer.

Grasso, M., Colosimo, B.M., 2017. Process defects and in situ monitoring methods in metal powder bed fusion: A review. Measur. Sci. Technol. 28, 044005. http://dx.doi.org/10.1088/1361-6501/aa5c4.

Grenestedt, J.L., 2005. On interactions between imperfections in cellular solids. J. Mater. Sci. 40, 5853–5857. http://dx.doi.org/10.1007/s10853-005-5019-4f.

Gross, A., Pantidis, P., Bertoldi, K., Gerasimidis, S., 2019. Correlation between topology and elastic properties of imperfect truss-lattice materials. J. Mech. Phys. Solids 124, 577–598. http://dx.doi.org/10.1016/j.jmps.2018.11.007.

Guest, S., Hutchinson, J., 2003. On the determinacy of repetitive structures. J.Mech. Phys. Solids 51, 383–391. http://dx.doi.org/10.1016/S0022-5096(02)00107-2.

Guo, X., Gibson, L.J., 1999. Behavior of intact and damaged honeycombs: A finite element study. Int. J. Mech. Sci. 41, 85–105. http://dx.doi.org/10.1016/S0020-7403(98)00037-X.

Guo, X.D.E., McMahon, T.A., Keaveny, T.M., Hayes, W.C., Gibson, L.J., 1994. Finite element modeling of damage accumulation in trabecular bone under cyclic loading. J. Biomech. 27, 145–155. http://dx.doi.org/10.1016/0021-9290(94)90203-8.

Gurtner, G., Durand, M., 2014. Stiffest elastic networks. Proc. Royal Soc. A 470, 20130611. http://dx.doi.org/10.1016/0021-9290(94)90203-8.

Hashin, Z., 1965. On elastic behaviour of fibre reinforced materials of arbitrary transverse phase geometry. J. Mech. Phys. Solids 13, 119–134. http://dx.doi.org/10.1016/0022-5096(65)90015-3.

Hashin, Z., Shtrikman, S., 1963. A variational approach to the theory of the elastic behaviour of multiphase materials. J. Mech. Phys. Solids 11, 127–140. http://dx.doi.org/10.1016/0022-5096(63)90060-7.

Hutchinson, R., Fleck, N., 2006. The structural performance of the periodic truss. J. Mech. Phys. Solids 54, 756–782. http://dx.doi.org/10.1016/j.jmps.2005.10.008.

Hutchinson, R., Wicks, N., Evans, A., Fleck, N., Hutchinson, J., 2003. Kagome plate structures for actuation. Int. J. Solids Struct. 40, 6969–6980. http://dx.doi.org/10.1016/S0020-7683(03)00348-2, Special issue in Honor of George J. Dvorak.

Hyun, S., Torquato, S., 2002. Optimal and manufacturable two-dimensional, Kagomé-like cellular solids. J. Mater. Res. 17, 137–144. http://dx.doi.org/10.1557/JMR.2002.0021.

Jenett, B., Calisch, S., Cellucci, D., Cramer, N., Gershenfeld, N., Swei, S., Cheung, K.C., 2017. Digital morphing wing: Active wing shaping concept using composite lattice-based cellular structures. Soft Robot. 4, 33–48. http://dx.doi.org/10.1089/soro.2016.0032.

Li, K., Gao, X.L., Subhash, G., 2005. Effects of cell shape and cell wall thickness variations on the elastic properties of two-dimensional cellular solids. Int. J. Solids Struct. 42, 1777–1795. http://dx.doi.org/10.1016/j.ijsolstr.2004.08.005.

Liu, L., Kamm, P., García-Moreno, F., Banhart, J., Pasini, D., 2017. Elastic and failure response of imperfect three-dimensional metallic lattices: the role of geometric defects induced by selective laser melting. J. Mech. Phys. Solids 107, 160–184. http://dx.doi.org/10.1016/j.jmps.2017.07.003.

Lu, Z.X., Liu, Q., Huang, J.X., 2011. Analysis of defects on the compressive behaviors of open-cell metal foams through models using the FEM. Mater. Sci. Eng. A 530, 285–296. http://dx.doi.org/10.1016/j.msea.2011.09.088.

Maxwell, J.C., 1864. On the calculation of the equilibrium and stiffness of frames. Lond. Edinb. Dublin Philos. Mag. J. Sci. 27, 294–299. http://dx.doi.org/10.1080/14786446408643668.

McHale, C., Hadjiloizi, D.A., Weaver, P.M., 2021. Toroidal deployment of morphing cylindrical lattices. Compos. Struct. 276, 114577. http://dx.doi.org/10.1016/j.compstruct.2021.114577.

Melancon, D., Bagheri, Z., Johnston, R., Liu, L., Tanzer, M., Pasini, D., 2017. Mechanical characterization of structurally porous biomaterials built via additive manufacturing: Experiments, predictive models, and design maps for load-bearing bone replacement implants. Acta Biomater. 63, 350–368. http://dx.doi.org/10.1016/j.actbio.2017.09.013.

Mertens, R., Clijsters, S., Kempen, K., Kruth, J.P., 2014. Optimization of scan strategies in selective laser melting of aluminum parts with downfacing areas. J. Manuf. Sci. Eng. 136, http://dx.doi.org/10.1115/1.4028620.

Namasivayam, U.M., Seepersad, C.C., 2011. Topology design and freeform fabrication of deployable structures with lattice skins. Rapid Prototyp. J. 17, 5–16. http://dx.doi.org/10.1108/13552541111098581.

Nelissen, W., Ayas, C., Tekoğlu, C., 2019. 2D lattice material architectures for actuation. J. Mech. Phys. Solids 124, 83–101. http://dx.doi.org/10.1016/j.jmps.2018.09.035.

Olympio, K.R., Gandhi, F., 2010. Flexible skins for morphing aircraft using cellular honeycomb cores. J. Intell. Mater. Syst. Struct. 21, 1719–1735. http://dx.doi.org/10.1177/1045389X09350331.

Onck, P., Merkerk, R., Raaijmakers, A., De Hosson, J., 2005. Fracture of open- and closed-cell metal foams. J. Mater. Sci. 40, 5821–5828. http://dx.doi.org/10.1007/s10853-005-4996-7.

Pellegrino, S., Calladine, C., 1986. Matrix analysis of statically and kinematically indeterminate frameworks. Int. J. Solids Struct. 22, 409–428. http://dx.doi.org/10.1016/0020-7683(86)90014-4.

Pronk, T., Ayas, C., Tekoğlu, C., 2017. A quest for 2D lattice materials for actuation. J. Mech. Phys. Solids 105, 199–216. http://dx.doi.org/10.1016/j.jmps.2017.05.007.

Romijn, N.E., Fleck, N.A., 2007. The fracture toughness of planar lattices: Imperfection sensitivity. J. Mech. Phys. Solids 55, 2538–2564. http://dx.doi.org/10.1016/j.jmps.2007.04.010.

Silva, M.J., Gibson, L.J., 1997. The effects of non-periodic microstructure and defects on the compressive strength of two-dimensional cellular solids. Int. J. Mech. Sci. 39, 549–563. http://dx.doi.org/10.1016/S0020-7403(96)00065-3.

Sun, J., Guan, Q., Liu, Y., Leng, J., 2016. Morphing aircraft based on smart materials and structures: A state-of-the-art review. J. Intell. Mater. Syst. Struct. 27, 2289–2312. http://dx.doi.org/10.1177/1045389X16629569.

Symons, D., Fleck, N., 2008. The imperfection sensitivity of isotropic two-dimensional elastic lattices. J. Appl. Mech. 75, http://dx.doi.org/10.1115/1.2913044.

Symons, D., Shieh, J., Fleck, N., 2005. Actuation of the Kagome double-layer grid. Part 2: Effect of imperfections on the measured and predicted actuation stiffness. J. Mech. Phys. Solids 53, 1875–1891. http://dx.doi.org/10.1016/j.jmps.2005.02.008.

Tankasala, H., Deshpande, V., Fleck, N., 2017. Tensile response of elastoplastic lattices at finite strain. J. Mech. Phys. Solids 109, 307–330. http://dx.doi.org/10.1016/j.jmps.2017.02.002.

Wallach, J., Gibson, L., 2001. Defect sensitivity of a 3D truss material. Scr. Mater. 45, 639–644. http://dx.doi.org/10.1016/S1359-6462(01)01073-9.

Wicks, N., Guest, S., 2004. Single member actuation in large repetitive truss structures. Int. J. Solids Struct. 41, 965–978. http://dx.doi.org/10.1016/j.ijsolstr.2003.09.029.

Yan, C., Hao, L., Hussein, A., Raymont, D., 2012. Evaluations of cellular lattice structures manufactured using selective laser melting. Int. J. Mach. Tools Manuf. 62, 32–38. http://dx.doi.org/10.1016/j.ijmachtools.2012.06.002.